Comprehensive Survey and Assessment of Spacecraft Relative Motion Dynamics Models

Joshua Sullivan,* Sebastian Grimberg,† and Simone D'Amico‡
Space Rendezvous Laboratory, Stanford University, Stanford, California 94305-4035

DOI: 10.2514/1.G002309

I. Introduction

IN THE framework of spacecraft relative motion, current dynamics models are diverse and often subject to a multitude of constraints and limitations on the intersatellite range of applicability, the eccentricity of the satellite orbits, the type of modeled perturbation forces, and the degree of computational effort required for propagation. Accordingly, it can be difficult to establish a benchmark to determine which dynamics models are applicable for a given mission scenario and to assess the efficacy of newly developed relative motion solutions. The intent of this paper is to provide an extensive survey of the currently available literature on closed-form relative motion dynamics models, highlighting the distinctions between various approaches and their contributions to the overall field of study. Closed-form analytical models are considered because they provide a compact and efficient capability to propagate the relative motion dynamics that does not require numerical integration of the equations of motion, lending themselves to useful applications in both onboard guidance, navigation, and control (GN&C) systems as well as offline mission-planning analysis. Particular attention is paid to the dynamical state representation, the immediate assumptions on the model, the types of perturbations included, and the provided metrics on accuracy and computational complexity. This survey additionally seeks to harmonize the connection between models of different state spaces through an evaluation of their respective interrepresentation mappings. Finally, a comparative assessment of a subset of surveyed dynamics models is conducted to provide quantitative metrics for model performance subject to consistent test conditions that emulate realistic relative motion scenarios. The effects of reference orbit eccentricity, interspacecraft separation, and the inclusion of relevant perturbations are dissected through a simulation-based evaluation of the closed-form dynamics

Joshua Sullivan is a Ph.D. candidate working in the Space Rendezvous Laboratory (SLAB) at Stanford University. He received his B.S. degree from the University of California, San Diego and his M.S. degree from Stanford University, both in aerospace engineering. He has experience working as an engineering analyst for SpaceX and Space Systems/Loral. His current research focuses on developing advanced algorithms for angles-only relative navigation and rendezvous in distributed space systems as well as formulating improved analytical dynamics models for orbital relative motion.

Sebastian Grimberg is a Master's student working in the SLAB at Stanford University. He graduated with a Bachelor of Science in Engineering in mechanical and aerospace engineering and a certificate in engineering physics from Princeton University in 2015. His current research focus is in the field of dynamics models for orbital relative motion, specifically the development of accurate and computationally efficient semi-analytical methods to propagate the relative state in a wide range of orbit scenarios.

Simone D'Amico is an Assistant Professor of Aeronautics and Astronautics at Stanford University, a Terman Faculty Fellow of the School of Engineering, Founder and Director of the Space Rendezvous Laboratory, and Satellite Advisor of the Student Space Initiative, Stanford's largest undergraduate organization. He received his B.S. and M.S. from Politecnico di Milano and his Ph.D. from Delft University of Technology. Before Stanford, Dr. D'Amico was at DLR, German Aerospace Center, where he gave key contributions to the design, development, and operations of spacecraft formation-flying and rendezvous missions such as GRACE (United States/Germany), TanDEM-X (Germany), and PRISMA (Sweden/Germany/France), for which he received several awards. Dr. D'Amico's research lies at the intersection of advanced astrodynamics, GN&C, and space system engineering to enable future distributed space systems. He has over 100 scientific publications including conference proceedings, peer-reviewed journal articles, and book chapters. He has been a Programme Committee Member (2008), Co-Chair (2011), and Chair (2013) of the International Symposium on Spacecraft Formation Flying Missions and Technologies. He is a Programme Committee Member of the International Workshop on Satellite Constellations and Formation Flying since 2013. He is Associate Editor of the *Journal of Guidance, Control, and Dynamics* and the *Journal of Space Science and Engineering*.

Received 23 June 2016; revision received 3 January 2017; accepted for publication 19 January 2017; published online 12 April 2017.

*Doctoral Candidate, Department of Aeronautics and Astronautics, Durand Building, 496 Lomita Mall.
†Graduate Student, Department of Aeronautics and Astronautics, Durand Building, 496 Lomita Mall.
‡Assistant Professor, Director of the Space Rendezvous Laboratory, Department of Aeronautics and Astronautics, Durand Building, 496 Lomita Mall.

models against multiple numerically propagated force models. Such a survey is not currently available in the literature, and its introduction provides a comprehensive resource that focuses on pragmatic model features such as the assumptions on orbit geometry or the inclusion of perturbations as well as ways by which the merits of individual methods can be connected to other models to form a more replete understanding of the relative motion dynamics.

As a matter of terminology, the relative dynamics model seeks to describe the motion of a spacecraft, denoted as the deputy, with respect to a reference spacecraft, denoted as the chief. Note that, without loss of generality, the chief could also define an ideal reference orbit or trajectory instead of the physical orbit of a spacecraft. It is important to note that this survey addresses relative motion with respect to a closed chief orbit about Earth in the context of the two-body problem. As such, dynamics models describing the relative motion about the Lagrange points or near-Earth objects are not discussed.

A preliminary examination of existing literature surveys in relevant scientific fields was conducted to determine the appropriate structural and stylistic portrayal of the diverse content of this topic. In particular, this work takes inspiration from the concise yet cogent surveying done by Scharf et al. [1,2] and Alfriend and Yan [3], both for their relevance to the field of spacecraft formation-flying and for their efforts in logically structuring the survey to capture a multitude of information in a short format. The work by Russell [4] and Quadrelli et al. [5] instead provides clear examples of lengthier and thoroughly detailed literature surveys that could very well act as standalone introductions to the topics being discussed. This paper seeks to strike a balance between these two styles, offering a concise but detailed standalone survey that captures the state of the art in the field of spacecraft relative dynamics. It also serves as an introduction to future work in the improvement of existing models.

At the broadest level, the current work on relative motion dynamics can be categorized by the state representation used to parameterize the relative motion. Accordingly, Sec. II discusses models that use a translational representation of the relative state vector, such as the relative position and velocity of the deputy relative to the chief expressed in rectilinear or curvilinear coordinates. Section III instead focuses on dynamics models parameterized by orbital element-based states, where the relative state is made up of linear or nonlinear combinations of the chief and deputy orbital elements. Within these broad groups, the relative dynamics models are further characterized by the reference orbit regime of applicability, namely the case of near-circular orbits or orbits of arbitrary eccentricity. Additionally, a distinction is made between nonlinear models and those that employ a linearization assumption of small spacecraft separation with respect to the reference spacecraft orbital radius. Section IV examines the relevant mappings between representations and relationships between the considered dynamics models in these first two state categories. Relevant state representations that do not fit neatly into the aforementioned two categories are then explored in Sec. V. Section VI describes a comparative assessment that is conducted to evaluate the performance of a subset of the surveyed dynamics models subject to several test scenarios and validated against high-fidelity numerical force models. Finally, Sec. VII offers closing remarks on the surveying outcomes and comparative assessment results. A thorough tabular summary of the surveyed dynamics models is given in Appendix A, and a detailed overview of several of the mappings between representations is provided in Appendix B.

II. Dynamics Models Using a Translational State Representation

The most elementary and historically studied parameterization of relative motion uses the relative position $\boldsymbol{\rho} = (x, y, z)^T$ and velocity $\dot{\boldsymbol{\rho}} \triangleq {}^{\mathcal{R}}\mathrm{d}\boldsymbol{\rho}/\mathrm{d}t = (\dot{x}, \dot{y}, \dot{z})^T$ of the deputy defined in a rotating reference frame $\mathcal{R}$ centered on the chief, resulting in the six-dimensional relative state vector $\delta\boldsymbol{x} = (\boldsymbol{\rho}, \dot{\boldsymbol{\rho}})^T$. This so-called chief rotating RTN frame is composed of orthogonal basis vectors where $\hat{\boldsymbol{R}}$ is directed along the chief position vector, $\hat{\boldsymbol{N}}$ is in the direction of the chief orbital angular momentum vector, and $\hat{\boldsymbol{T}} = \hat{\boldsymbol{N}} \times \hat{\boldsymbol{R}}$ completes the right-handed triad. Note that ${}^{\mathcal{R}}\mathrm{d}(\cdot)/\mathrm{d}t$ denotes the derivative with respect to time, taken in the rotating reference frame.

An extensive derivation is conducted by Alfriend et al. [6], where the equations of relative motion are obtained by expressing the relative acceleration of the deputy in the chief RTN frame, resulting in the general nonlinear equations of relative motion

$$\begin{aligned}
\ddot{x} - 2\dot{f}_c\dot{y} - \ddot{f}_c y - \dot{f}_c^2 x &= -\frac{\mu(r_c + x)}{[(r_c + x)^2 + y^2 + z^2]^{3/2}} + \frac{\mu}{r_c^2} + d_R \\
\ddot{y} + 2\dot{f}_c\dot{x} + \ddot{f}_c x - \dot{f}_c^2 y &= -\frac{\mu y}{[(r_c + x)^2 + y^2 + z^2]^{3/2}} + d_T \\
\ddot{z} &= -\frac{\mu z}{[(r_c + x)^2 + y^2 + z^2]^{3/2}} + d_N
\end{aligned} \tag{1}$$

with time as the independent variable. Here, f_c denotes the chief true anomaly, r_c denotes the chief radius, and $\boldsymbol{d} = \boldsymbol{d}_d - \boldsymbol{d}_c = (d_R, d_T, d_N)^T$ is the differential perturbing acceleration vector representing forces other than spherical Earth gravity acting on the spacecraft expressed in the chief RTN frame. In this paper, the subscripts c and d refer to chief and deputy spacecraft quantities, respectively.

A. Near-Circular Reference Orbit

Under the assumption of a circular reference orbit, the angular velocity of the chief frame, $\dot{f}_c$, is the constant chief mean motion, n_c, and Eq. (1) becomes autonomous and simpler. The following models are developed using this fundamental assumption, but they are often implemented in cases where the chief eccentricity is very small but nonzero.

1. *Linear Models*

In the framework of spacecraft rendezvous, Clohessy and Wiltshire [7] derive a linear form of the equations of relative motion by retaining only first-order terms in the Taylor expansion of the nonlinear differential gravity and neglecting all other perturbations in Eq. (1). These equations of motion, known as the Hill–Clohessy–Wiltshire (HCW) equations, have a simple closed-form state transition matrix (STM) solution characterized by decoupled in-plane cycloidal motion and out-of-plane harmonic motion. The HCW equations have been used extensively since the 1960s for spacecraft close-proximity operations modeling, with flight heritage on the manned Gemini, Apollo, and Shuttle missions (NASA) [8–10], the XSS-10 and -11 on-orbit servicing technology demonstrations (Air Force Research Laboratory) [11], the autonomous ETS-VII (Japanese Aerospace Exploration Agency) [12], and others.

Although the initial formulation considers rectilinear relative position and velocity, more recent investigations discussed by Alfriend et al. [6] and De Bruijn et al. [13] show that an identical form of the HCW equations can be formulated using a curvilinear relative state. This representation intrinsically better captures the orbit curvature, leading to improvements in the computation of the initial conditions and thus in model accuracy. Indeed, results presented in [13] reveal that using the curvilinear HCW equations delivers position propagation errors that are orders of magnitude better than the rectilinear implementation when the relative separation is largely in the along-track direction, with perfect Keplerian relative motion prediction in the case of purely along-track separation.

Instead of describing the relative motion directly through position and velocity components, Lovell and Tragesser [14] and Chavez and Lovell [15] use a change of coordinates to establish a state built from the integration constants of the HCW solution. In their research studies, the authors demonstrate the improved geometric insight and guidance control simplicity afforded by working with these new HCW invariant parameters but do not develop a framework for including other perturbations. Additional examples of parameterizing the relative motion with invariant trajectory parameters are provided by Ichikawa and Ichimura [16] in the context of relative orbit transfer using the HCW equations as well as by Healy and Henshaw [17], who define a set of geometric relative orbital parameters that are analogous to the classical orbital elements. The

latter provide a detailed methodology for computing the geometric parameters based on constraints imposed by the unperturbed relative motion, and just as [14], provide a compelling argument for the simplicity and geometric insight provided by the new relative motion description through straightforward impulsive maneuvers to reconfigure the orbital parameters.

In response to the lack of perturbations considered in the HCW solution, Schweighart and Sedwick [18] and Izzo et al. [19] derive extensions of the model to incorporate first-order effects of the Earth oblateness J_2 perturbation. Developments in [18] correct for first-order J_2 effects on the reference orbital period and nodal drift and present numerical results indicating position modeling errors at the meter level when compared with a numerical integration of the absolute J_2-perturbed equations of motion. Although Izzo et al. [19] do not initially consider the effect of J_2 on the chief orbit, the authors do include first-order perturbing accelerations due to atmospheric drag in the extension of the HCW model. The ensuing analysis uses Floquet theory to predict a slowly manifesting relative motion instability due to the considered perturbations, consistent with the presented simulation results. Izzo [20] later expanded the research to consider the perturbation of the reference frame angular velocity but did not arrive at closed-form solutions.

Early work by Leonard et al. [21] examines the use of the HCW dynamics model in conjunction with differential drag acting as a constant acceleration in the antiflight direction. By imposing a simple coordinate transformation to describe the relative motion with respect to an average position of the unperturbed equations, the perturbed equations result in two uncoupled second-order differential equations, for which the authors demonstrate closed-form control laws for formation-keeping. Humi and Carter [22] and Carter and Humi [23] develop extensions of the HCW analytical solution to incorporate the effect of atmospheric drag on two spacecraft flying in formation. In [22], a linear drag model is considered where the drag force varies proportionally with the velocity. Carter and Humi [23] improve this formulation by considering a quadratic drag model, where force varies with the square of spacecraft velocity. It is important to note that, to simplify the solution, the authors assume an atmospheric density profile that varies inversely with altitude and that both spacecraft have identical ballistic coefficients. The result is a modified version of the HCW STM that includes the effect of atmospheric drag on the relative motion in the radial direction. In more recent work, Bevilacqua and Romano [24] develop a method for using atmospheric drag to conduct rendezvous maneuvers with multiple spacecraft in near-circular orbits by adopting the original approach of Leonard et al. [21]. The analytical control design uses a J_2-perturbed dynamic model built from the aforementioned Schweighart–Sedwick solution that is improved to incorporate the drag-based maneuvers.

With respect to the aforementioned work of Lovell and Tragesser, research by Bevilacqua and Lovell [25] presents a new analytical solution for the evolution of the relative state subject to continuous thrust. The authors establish the practical merit of this new formulation by incorporating orbital rephasing and rendezvous maneuvers designed using input shaping theory. Similarly, Bennett and Schaub [26] develop a set of variational equations for the relative state developed by Lovell and Tragesser using a Lagrange bracket formulation that captures the evolution of the state parameters due to perturbing accelerations expressed in the chief RTN frame. The resulting model is used to design closed-form control policies subject to this perturbation. Finally, it is important to mention the work of Colombo [27], which provides an analytical solution to the HCW model while including constant and once-per-orbit harmonic empirical accelerations in the radial, along-track, and cross-track components. The framework developed in that work can be used to model a multitude of perturbations that manifest as a superposition of constant and harmonic accelerations occurring at the orbital angular rate.

2. *Nonlinear Models*

For relative motion considerations where the previous linearization assumption breaks down, several authors have directly considered the simplified autonomous nonlinear equations of relative motion under the circular chief orbit assumption. In this context, the assumption of small interspacecraft separation is relaxed to obtain new closed-form solutions to the equations of relative motion. The analysis of Newman et al. [28] provides a detailed comparative assessment of six relevant nonlinear solutions explored by multiple authors, namely the quadratic Volterra (QV) in rectilinear coordinates, the multiple scales (MS) in spherical coordinates, the double transformation (DT) in cylindrical and spherical coordinates, and the approximated double transformation (A-DT) in cylindrical and spherical coordinates.

The quadratic Volterra solution uses an expansion of the Volterra series built from the nonlinear two-body orbital equations of motion to form the solution in terms of linear, bilinear, and quadratic expressions of the rectilinear initial conditions. The derived solution offers improved geometric insight into the nonlinear effects on the relative motion, namely through previously unmodeled bias terms and new higher-frequency oscillatory terms. Additionally, the quadratic Volterra solution reveals new secular terms that change the along-track drift rate and introduce drift in the radial and cross-track directions. For Keplerian motion, the presence of radial and cross-track drift is nonphysical, and accordingly, the quadratic Volterra model is limited to applications with short time scales. A framework for including the J_2 perturbation in the quadratic Volterra method is developed by Stringer et al. [29], but the ensuing derivations neglect perturbations for simplification. The multiple-scales solution makes use of the multiple-scales perturbation technique to capture solutions up to second order using spherical coordinates. Although the resulting expressions have some terms consistent with the quadratic Volterra, the multiple-scales solution removes nonphysical radial and cross-track drifts present in the quadratic Volterra solution. Unlike the previous two approaches, the double transformation and approximated double transformation do not produce perturbation solutions from series expansions. Instead, the double transformation solution uses the nonlinear mapping between cylindrical (or spherical) coordinates and rectilinear coordinates to rewrite the cylindrical (or spherical) HCW solution in terms of the nonlinear combination of rectilinear initial conditions. The approximated double transformation methods retain nonlinear terms only up to second order from the associated double transformation results. In this way, the double transformation and approximated double transformation models build a solution from the linear HCW model that is nonlinear in the initial conditions.

Numerical simulation results show that the quadratic Volterra method is much more accurate than the other solutions in the case of small along-track separations, with propagation errors at the submeter level with respect to a two-body motion numerical integration force model. Instead, the double transformation-based and multiple-scales solutions outperform for large along-track separations due to their use of curvilinear coordinates, with demonstrated accuracy at the submeter level. The authors highlight that the double transformation and multiple-scales models are subject to persistent but slowly drifting error due to only retaining the linear HCW along-track drift term, whereas the quadratic Volterra predicts additional drifting motion in the other directions. Additional work by Perez et al. [30] extends the comparison of the double transformation and quadratic Volterra solutions to more simulated test cases, further concluding that the quadratic Volterra is more accurate when there is relative motion in the cross-track direction but that the double transformation solution offers comparable accuracy for most cases with the added benefit of a simpler implementation. It is important to note that, although these nonlinear models extend the intersatellite range of applicability by capturing higher-order separation effects, they neglect the potentially larger effects of chief orbit eccentricity entirely.

B. Arbitrarily Eccentric Reference Orbit

In the case where the reference orbit is not assumed to be circular, the chief angular velocity $\dot{f}_c$ is no longer constant, and Eq. (1) is time-varying. Existing approaches in the literature differ in the

independent variable used to parameterize this variation, with the majority of work seeking either a true-anomaly-explicit solution or a time-explicit solution.

1. Linear Models Using True Anomaly as the Independent Variable

In research conducted by Lawden [31] as well as Tschauner and Hempel [32], the linear forms of the equations of relative motion in arbitrarily eccentric orbit are derived by retaining only first-order terms in the Taylor expansion of the nonlinear differential gravity perturbation from Eq. (1). These so-called Tschauner–Hempel (TH) equations are characterized by derivatives taken with respect to the reference true anomaly and display a decoupling of the in-plane and out-of-plane equations consistent with the previous HCW model. Although the out-of-plane harmonic motion was immediately tractable, Lawden's original solution for the coupled in-plane motion displays singularities at chief perigee and apogee, thus prompting subsequent improvements by several authors.

Carter [33] addresses the singularity issues present in Lawden's original solution by making use of a modified fundamental integral solution to the coupled in-plane equations of motion. The resulting STM is proven to be singularity-free, albeit computationally complex, and no performance metrics are given. Instead, the developments outlined by Yamanaka and Ankersen [34] use a different fundamental integral solution written in terms of Kepler's equation to construct an STM that is structurally simpler and no longer prone to singularities. For these reasons, the Yamanaka–Ankersen STM is generally considered the state-of-the-art solution for linear propagation of the relative position and velocity in eccentric orbit and will be used on the proposed Proba-3 (European Space Agency) solar coronagraph formation [35] flying in highly elliptical orbit. Unlike in [33], the Yamanaka–Ankersen model [34] was verified against a numerical integration of the nonlinear equations of two-body orbital motion as well as the HCW model. Simulation results presented by Yamanaka and Ankersen for reference orbits with a 500 km perigee altitude and eccentricity values of 0.1 and 0.7 show a strong agreement of their model with the numerical integration, whereas the HCW model completely breaks down, as expected.

2. Linear Models Using Time as the Independent Variable

The following surveyed methods do not attempt a solution to the TH equations but rather seek solutions parameterized by time as the independent variable. A common feature among the highlighted models is the use of the analytical solution to the two-body unperturbed problem developed by Battin [36].

The method proposed by Melton [37] captures the linearized equations of motion in a time-varying cylindrical state-space plant matrix. Higher-order eccentricity effects are retained by rewriting the equations of motion in terms of the chief radius and angular velocity expanded in powers of eccentricity. The resulting STM takes on a similar expansion in powers of eccentricity, with higher-order elements computed as recursive integral expressions from lower-order elements. A comparison of the proposed model for reference orbits with eccentricity as high as 0.3 indicates that retaining up to second-order eccentricity terms in the STM improves the modeling performance by about 300% when compared with lower-order models.

In contrast, Broucke [38] develops a solution to the linear de Vries equations [39] describing elliptical motion in a rotating coordinate frame. The proposed model uses the analytical solution from Battin to express the cylindrical in-plane STM components as variations of the chief radius and velocity with respect to the orbital element parameters a, e, ω, M_0 (i.e., the chief semimajor axis, eccentricity, argument of periapsis, and initial mean anomaly). Similarly, the work of Lee, Cochran, and Jo (LCJ) [40] establishes a linear map between the relative motion state and the variation of the chief in-plane position and velocity, inclination i, and right ascension of the ascending node (RAAN, Ω). The proposed LCJ STM is constructed by applying this map as a similarity transformation to the sensitivity matrix of the chief motion with respect to the initial chief state resulting from Battin's solution. Numerical simulation tests reveal relative position and velocity modeling errors of approximately 70 m and 0.1 $\mathrm{m}\cdot\mathrm{s}^{-1}$, respectively, after two orbits at an eccentricity of 0.4 and perigee altitude of 500 km using the LCJ STM. The authors claim that improvements can be achieved using a smaller simulation step size, but no metrics are provided in the publication.

3. Nonlinear Models

Kechichian [41] derives a set of nonlinear differential equations that describe the dynamics of a satellite with respect to a chief reference frame that is "dragging" due to aerodynamic effects and "precessing" due to the J_2 perturbation. To mitigate the complexity of Kechichian's original formulation, Theron et al. [42] highlight an improved derivation procedure by expanding the relative acceleration in terms of absolute orbital elements and applying the Lagrange osculating condition to the J_2-perturbed equations. Although the authors do not introduce drag effects as Kechichian did, they do incorporate the differential perturbation due to thrusting maneuvers. These two particular sets of relative motion equations can be considered a subset of the general nonlinear Eq. (1), valid under exposure to the aforementioned perturbations included in their derivation. Neither publication offers closed-form solutions to the derived nonlinear equations of motion, but Theron et al. [42] do provide numerical integration results, which show relative position and velocity errors within 2.5% of the true model for reference orbits with a perigee altitude of 600 km and eccentricity of 0.5.

III. Dynamics Models Using an Orbital Element State Representation

Several authors have sought to obtain simpler and higher-fidelity solutions to the relative motion problem by describing the relative dynamics using a state based on the orbital elements that specify the chief and deputy orbits. Here, the relative orbital elements (ROE) are defined as a set of six unique linear or nonlinear combinations of the chief and deputy absolute orbital elements. An ROE-based state benefits from the slowly time-varying nature of the absolute orbital elements and enables the use of the Lagrange planetary equations (LPE) and Gauss variational equations (GVE) to include orbital perturbations and control maneuvers in the relative motion problem.

The choice of a relative orbital element state defines a function $\boldsymbol{f}(\boldsymbol{\alpha}_c, \boldsymbol{\alpha}_d)$, which returns the relative state $\delta\boldsymbol{\alpha}$, given a set of chief and deputy orbital elements $\boldsymbol{\alpha}_c$ and $\boldsymbol{\alpha}_d$, respectively. Additionally, the well-documented GVE provides analytical expressions for the time evolution of the osculating absolute orbital elements subject to a general perturbing acceleration. In equation form,

$$\delta\boldsymbol{\alpha} = \boldsymbol{f}(\boldsymbol{\alpha}_c, \boldsymbol{\alpha}_d)$$
$$\frac{\mathrm{d}\boldsymbol{\alpha}_c}{\mathrm{d}t} = \boldsymbol{G}(\boldsymbol{\alpha}_c)\boldsymbol{d}_c \quad \text{and} \quad \frac{\mathrm{d}\boldsymbol{\alpha}_d}{\mathrm{d}t} = \boldsymbol{G}(\boldsymbol{\alpha}_d)\boldsymbol{R}_c^d\boldsymbol{d}_d \tag{2}$$

captures these relevant relationships, where $\boldsymbol{G}$ is the matrix defining the time derivatives of the osculating absolute orbital elements via the GVE, and $\boldsymbol{R}_c^d$ is the rotation matrix from the chief RTN frame to that of the deputy. As was the case for Eq. (1), the perturbing accelerations on the chief and deputy have been expressed in the RTN frame of the chief. Then, the time derivative of the ROE, which expresses the dynamical equations governing the relative motion, is given as

$$\frac{{}^{\mathcal{R}}\mathrm{d}\delta\boldsymbol{\alpha}}{\mathrm{d}t} = \frac{\partial \boldsymbol{f}(\boldsymbol{\alpha}_c, \boldsymbol{\alpha}_d)}{\partial \boldsymbol{\alpha}_c}\boldsymbol{G}(\boldsymbol{\alpha}_c)\boldsymbol{d}_c + \frac{\partial \boldsymbol{f}(\boldsymbol{\alpha}_c, \boldsymbol{\alpha}_d)}{\partial \boldsymbol{\alpha}_d}\boldsymbol{G}(\boldsymbol{\alpha}_d)\boldsymbol{R}_c^d\boldsymbol{d}_d \tag{3}$$

The following sections examine several relative motion models that use this general orbital element-based form of the state vector.

A. States Based on Mean Orbital Element Differences

One common state choice is to define the ROE as the arithmetic difference between deputy and chief orbital elements, such that $\delta\boldsymbol{\alpha} = \Delta\boldsymbol{\alpha} = \boldsymbol{\alpha}_d - \boldsymbol{\alpha}_c$. This relative state parameterization is used

extensively by Schaub [43] and is usually denoted as the orbital element differences (OEDs) or differential orbital elements. In this paper, the term OED will be used exclusively to refer to the arithmetic difference of orbital elements. It is emphasized that $\Delta(\cdot)$ defines the arithmetic difference operator and is not to be confused with the notation of $\delta(\cdot)$, specifying a relative quantity to distinguish it from an absolute quantity. In the case of defining the ROE as OED, the $\delta(\cdot)$ and $\Delta(\cdot)$ signify the same quantities. For this parameterization of the relative state, the equations of relative motion in Eq. (3) simplify to

$$\frac{^{\mathcal{R}}\mathrm{d}\delta\boldsymbol{\alpha}}{\mathrm{d}t} = \boldsymbol{G}(\boldsymbol{\alpha}_d)\boldsymbol{R}_c^d\boldsymbol{d}_d - \boldsymbol{G}(\boldsymbol{\alpha}_c)\boldsymbol{d}_c \tag{4}$$

The absolute states may be specified in terms of six classical Keplerian, quasi-nonsingular, or fully nonsingular equinoctial orbital elements. The quasi-nonsingular orbital elements avoid singularities for circular orbits where the line of apsides is undefined, and the equinoctial orbital elements remove both circular and equatorial orbit singularities where neither the line of apsides nor the line of nodes is defined. A discussion of these orbital element variants can be found in [6].

To accommodate perturbations and formulate models for use in relative orbit design and control, many dynamical models use a relative state based on mean orbital elements instead of their osculating counterparts. The equations of relative motion in Eq. (3) or Eq. (4) give the exact evolution of the osculating ROE, and in general, their variation in time can be divided into short-period, long-period, and secular components. Through averaging theory or other approximations to the dynamics, the mean relative orbital elements can be defined, whose evolution includes the secular drift of their osculating counterparts but neglects the periodic oscillations. The difference between chief and deputy short-period oscillatory motion induced by perturbations generally decreases as the intersatellite separation decreases. Thus, although the secular variations due to J_2 are significant, the short-period effects can be reasonably neglected if the separation is within the range of validity for a linearization assumption. Additionally, control schemes based on mean orbital elements correct for the averaged effect of the perturbations from Keplerian motion without wasting fuel by compensating for short- and long-period variations.

1. *Linear Models*

Early work by Schaub and Alfriend [44] uses a relative state defined by Delaunay element differences derived from a J_2-perturbed Hamiltonian to explore relative orbits invariant to Earth oblateness perturbations. These passively stable J_2-invariant orbits are characterized by zero drift in the OED to first order. Similarly, the approaches of Schaub et al. [45,46] apply the specifications for J_2-invariance in development of continuous and impulsive control laws using the mean Delaunay OED to define the relative state vector.

The analytical model developed by Gim and Alfriend [47] captures both the effects of eccentricity and J_2 by leveraging Brouwer's solution [48] to the problem of satellite motion subject to higher-order geopotential perturbations. Although Brouwer's original method captures second-order secular and first-order periodic perturbations about a Keplerian reference orbit due to J_2 (in addition to secular and long-period effects of J_3–J_5), the Gim–Alfriend (GA) method retains only first-order secular J_2 terms. The core of the solution is an STM that was initially formulated to propagate a relative state of mean quasi-nonsingular OED, but subsequent improvements [49] have expressed the STM in terms of mean fully nonsingular OED. Note that the propagation of the mean quasi-nonsingular and fully nonsingular OED are not subject to singularities at the critical inclinations. These singularities will be discussed later in the context of osculating OED propagation. The Gim–Alfriend dynamics model was used in orbit design for the NASA MMS formation [50], studying magnetospheric phenomena in highly elliptical Earth orbit, and is used in the maneuver targeting algorithm forming the basis of the guidance system for NASA's cubesat proximity operations demonstration (CPOD) mission [51].

In more recent research efforts, Koenig et al. [52] generalize the derivation procedure for STM solutions that accommodate relevant perturbations such as J_2 and differential drag. First, making use of the GVE to express the time derivative of the ROE including perturbations, the ensuing first-order Taylor series expansion results in a linear dynamical plant matrix that is periodic and time-varying. Using Floquet theory, Koenig, Guffanti, and D'Amico (KGD) are able to transform the plant matrix into a compact STM (denoted here as the KGD STM) that is valid for arbitrarily eccentric reference orbits. Furthermore, this approach is developed for the singular, quasi-nonsingular, and fully nonsingular ROE states and can be generalized to incorporate any perturbations into ROE-based relative motion solutions.

2. *Nonlinear Models*

As a higher-accuracy extension of the earlier work in linear J_2-invariant relative orbits, a second-order nonlinear theory for relative motion dynamics based on mean Delaunay OED is developed by Alfriend [53] and Alfriend and Yan [54]. This so-called Yan–Alfriend nonlinear method is derived by expanding the mean OED time derivatives to second-order using a Taylor series about the chief orbit. This differs from the previous approach, which only considered linear OED terms of the Taylor expansion. The result is a nonlinear dynamics model for propagating the mean OED in arbitrarily eccentric orbits while including second-order J_2 effects. This method additionally offers second-order corrections to the conditions for J_2-invariant relative orbits derived in [44].

The aforementioned comparative work in [3] analyzes the relative performance of the Gim–Alfriend STM and the Yan–Alfriend nonlinear method as well as several translational state and lower-fidelity propagation models. The authors propose a modeling error index that captures the maximum error between the modeled and true reference state throughout propagation. This modeling error index becomes directly proportional to the percentage error for a one-dimensional state. Against a reference numerical integration including J_2, the modeling error index is examined under fixed separation for a range of eccentricity values and then for fixed eccentricity though a range of spacecraft separations. Ultimately, the authors conclude that the Yan–Alfriend method exhibits the highest propagation accuracy with a consistent error index of order 10^{-4} for separations up to 160 km. Instead, the Gim–Alfriend STM successfully accounts for chief eccentricity effects for a fixed separation but falls victim to linearization errors in the cases where that separation is large. The Gim–Alfriend modeling error index begins marginally larger than the Yan–Alfriend method at the smallest considered separation of 0.16 km but grows to two orders of magnitude larger at 160 km separation.

B. States Based on Relative Eccentricity and Inclination Vectors

The following discussion features dynamics models that use the quasi-nonsingular ROE, which contain the relative eccentricity and relative inclinations vectors. Although the initial implementation of the eccentricity and inclination vectors by Eckstein et al. [55] and Soop [56] was focused on the safe collocation of satellites in geostationary orbit (GEO), more recent research efforts have extended these applications to proximity operations in low Earth orbit (LEO) formations.

Arbinger et al. [57] use the eccentricity and inclination vector description for the precise absolute orbit control of the TerraSAR-X satellite about an osculating reference trajectory for synthetic aperture radar (SAR) interferometry applications. This technique is later extended to consider spacecraft relative motion in LEO, where the relative eccentricity and inclination vector formulation is used as the basis for the design and implementation of the safe longitude swap maneuver for the GRACE formation, which was required to balance environmental wear on the two spacecraft [58]. In that work, the relative eccentricity and inclination vectors are used to establish metrics of collision avoidance and passive safety based on the minimum formation separation in the plane perpendicular to the chief flight direction. This E/I-vector separation principle was later

fundamental to the orbit and control design of the TanDEM-X formation [59], which implemented the first on-orbit bistatic SAR to deliver the most accurate digital elevation modeling of Earth to date.

D'Amico [60] builds upon the previous work in [58,59] by developing a linear model for the relative dynamics that uses a state composed of the relative semimajor axis, the relative mean longitude, and the relative eccentricity and inclination vectors. The resulting STM captures the time-evolution of these quasi-nonsingular ROE subjects to first-order J_2 perturbations in near-circular, almost-bounded orbits. This formulation leads to practical closed-form solutions of the GVE, which are useful in developing straightforward control laws for formation-keeping that properly account for secular J_2 effects. The approach has been implemented on in-flight demonstrations of the TanDEM-X Autonomous Formation Flying system [61] and on the Spaceborne Autonomous Formation Flying Experiment during the PRISMA mission [62].

More recent work by Gaias et al. [63] using the same ROE state has improved upon the original J_2-perturbed STM developed in [60] by introducing the near-circular approximation later in the derivation and by including time-varying differential drag to formulate a new, more complete relative motion model. Although the original STM reveals a rotation of the relative eccentricity vector and a linear drift of the relative inclination vector as a function of the difference in inclination, the resulting J_2-perturbed STM from [63] (denoted here as the GAM STM) captures additional terms that describe the secular variation of the relative mean longitude and relative inclination vector as functions of the relative semimajor axis. The full model also describes mean variations of the relative eccentricity vector due to atmospheric density oscillations produced by day and night transitions. In numerical validation, results indicate that the new STM greatly outperforms the previous formulation in the case where there is a difference in semimajor axis between the two spacecraft. For the provided test case using a semimajor axis difference of 200 m, the previous STM from [60] poorly captures secular drifting of the relative mean longitude and y component of the relative inclination vector, with errors growing to tens of meters after 15 orbits, whereas the new model maintains submeter-level accuracy relative to the actual measured flight trajectory. Additionally, the authors confirm that, with their complete relative motion STM, which corrects these original J_2 formulation shortcomings and includes the effects of atmospheric drag, they are able to account for some of the numerical discrepancies seen in real flight data from phases of the PRISMA mission.

The GN&C strategies previously developed in [60] using the relative eccentricity and inclination vectors are extended to on-orbit servicing applications by Spurmann and D'Amcio [64] within the framework of the proposed DEOS mission (DLR, German Aerospace Center). In that work, the E/I-vector separation principle and the J_2-perturbed dynamics model developed in [60] are used to derive safe and flexible rendezvous profiles, given the expected accuracy of GPS navigation and radar tracking capabilities, as well as fuel-efficient formation-keeping control laws. As a major improvement to [64], the development of the AVANTI experiment [65] onboard the BIROS satellite of the FireBird mission (DLR) makes use of the recent STM [63] and maneuver-planning architecture [66,67] provided by Gaias et al. to compute impulsive maneuvers for Δv optimal ROE reconfiguration. In the same context, the guidance laws designed to maintain formation safety during the AVANTI experiment are based on determining the minimum radial/cross-track separation for any configuration of ROE parameters (i.e., nonzero relative semimajor axis as well as arbitrary phasing of the relative eccentricity and inclination vectors) [68].

The work of Spiridonova [69] further builds on the developments of [60,63] to model the dynamics of GEO formations for applications in on-orbit servicing. The author develops an extended relative dynamics model for near-circular orbits to include solar radiation pressure and third-body perturbations due to the sun and moon because they have a large effect on the relative motion at GEO altitudes. The complete propagation of the ROE state is given by first propagating the J_2-perturbed relative motion using the STM from [63] and then adding the derived effects of solar radiation pressure and third-body gravity to the relative state over the propagation time interval. In numerical simulation, the propagated ROEs are compared to a truth model resulting from numerical integration of the nonlinear equations of motion subject to high-order gravity, solar radiation pressure, and third-body effects. It is shown that the extended GEO model fully captures the secular drift in the ROE due to third-body perturbations and tracks the short- and long-period effects due to solar radiation pressure more closely than the original model from [63] considering only J_2 perturbations.

Of the previous research studies, only Gaias et al. [63] and Koenig et al. [52] include differential drag in the dynamics model. Although drag effects are of particular concern in low Earth orbit, it is has generally been a challenge to accurately model this perturbation for arbitrary formations because of the dependence on uncertain atmospheric density models, spacecraft geometry, and orientation. Instead, the methods proposed by Gaias et al. and Koenig et al. demonstrate that an empirical formulation is able to capture the mean effects of differential drag perturbations by augmenting the dynamical state with additional parameters describing the time derivative of the relative semimajor axis and relative eccentricity vector, which can be estimated in orbit (with constraints imposed by the observability of the scenario). Although in certain scenarios where differential drag is minimal, it may be beneficial to forgo incorporating a mismodeled effect, in situations where differential drag is a major perturbation, it is far better to include available models that are able to capture the mean effects accurately over daylong periods of time.

IV. Mapping Between Representations and Equivalence

It is important to reiterate that the aforementioned dynamics models provide a solution to a set of the governing differential equations of relative motion. Each model is subject to assumptions that define its applicability, such as orbit eccentricity, spacecraft separation, or inclusion of perturbations. Up to this point, the considered models have either parameterized the relative motion using rectilinear or curvilinear relative position and velocity (i.e., what has been denoted as translation state space) or using combinations of orbital elements. To understand the correspondence between solutions in the different state spaces, it is instructive to now consider the mappings between representations that are available in the literature.

The relative motion can be exactly determined by taking the difference between the deputy and chief absolute osculating orbital element-based solutions and expressing vectors in the appropriate reference frame. This results in a geometric mapping between the orbital elements of the chief and deputy and the translational relative state in RTN frame coordinates. This nonlinear mapping can be formulated as

$$\boldsymbol{\rho} = (x, y, z)^T = \boldsymbol{R}_I^c(\boldsymbol{\alpha}_c)\boldsymbol{r}_d(\boldsymbol{\alpha}_d) - (r_c, 0, 0)^T \tag{5}$$

where $\boldsymbol{r}_d(\boldsymbol{\alpha}_d)$ is the inertial position of the deputy written as a function of its absolute orbital elements, $\boldsymbol{R}_I^c(\boldsymbol{\alpha}_c)$ is the rotation matrix going from the inertial Earth-centered frame to the rotating chief-centered RTN frame, and the relative position $\boldsymbol{\rho}$ is expressed in the chief RTN frame as usual. The relative velocity $\dot{\boldsymbol{\rho}} \triangleq {}^{\mathcal{R}}\mathrm{d}\boldsymbol{\rho}/\mathrm{d}t$ comes directly from differentiating Eq. (5) with respect to time in the rotating chief RTN frame. The nonlinear transformation of absolute osculating orbital elements to absolute position and velocity, designated here as $\boldsymbol{r}(\boldsymbol{\alpha})$ and $\boldsymbol{v}(\boldsymbol{\alpha})$, respectively, is well-established; see for example Schaub and Junkins [70]. Given the chief absolute orbital elements and a set of ROEs, $\delta\boldsymbol{\alpha}$, the orbital elements of the deputy can be determined and used in Eq. (5) to transform the relative state in terms of orbital elements into the corresponding translational state equivalent. Note that Schaub and Junkins [70] also provide the appropriate functional inverses of $\boldsymbol{r}(\boldsymbol{\alpha})$ and $\boldsymbol{v}(\boldsymbol{\alpha})$. Accordingly, the inverse of Eq. (5) exists for mapping translational state variables to chief and deputy orbital elements.

Under appropriate assumptions, the nonlinear geometric transformation in Eq. (5) and its time derivative counterpart can be linearized and used to express the relationship between a ROE state and the relative position and velocity as the linear mapping

$$\delta\boldsymbol{x} = (\boldsymbol{\rho}, \dot{\boldsymbol{\rho}})^T \approx \boldsymbol{T}(\boldsymbol{\alpha}_c)\delta\boldsymbol{\alpha} \tag{6}$$

Sinclair et al. [71] provide a succinct discussion of the relationship shared between relative dynamics solutions expressed in different state representations. In particular, the authors highlight the fact that nonlinear relative motion solutions in translational state space and ROE space share an equivalence through their respective nonlinear mapping [Eq. (5)], and similarly, linear solutions share an equivalence through their respective linear transformations [Eq. (6)]. Although the surveyed dynamics models have largely been partitioned by state space, interrepresentation mappings provide the connection that allows us to take advantage of the solutions in each state representation without being constrained to one configuration space. To illustrate the merit of this concept, consider as an example the fact that the general translational state nonlinear equations of relative motion in Eq. (1) do not have a well-posed solution even in the unperturbed case. Instead, for unperturbed motion, the ROEs are generally slowly time-varying or constant, and the complete solution to Eq. (3) is rather simple. Thus, the relative state can be propagated in the ROE framework and mapped via Eq. (5) or Eq. (6) to an equivalent propagation of the translational state. Different forms of the nonlinear and linear mappings are discussed in detail in the following expositions.

A. Nonlinear Mappings

Gurfil and Kholshevnikov [72] develop the closed-form nonlinear scalar expressions resulting from Eq. (5). The authors introduce a relative RAAN, relative argument of periapsis, and relative inclination, which are related to the absolute orbital elements through spherical geometry. This introduction results in a simplified form of the equations for relative position in terms of orbital elements and these three new parameters. These equations are exact when using a state of osculating chief and deputy orbital elements, and they require solution of Kepler's equation to obtain an expression for the relative position as a function of time. The authors also note that the geometric structure of the problem resulting from the orbital elements parameterization yields the added benefit of a straightforward method to evaluate minimum, maximum, and mean separations between chief and deputy in a given relative orbit.

To obtain a time-series approximation to the relative position, Gurfil and Kasdin [73] use a series representation of Kepler's equation in terms of Bessel function expansions. The exact transformation expressing the relative position coordinates as nonlinear functions of the chief and deputy orbital elements [Eq. (5), now with time as the independent variable] are expanded in terms of the OED to arbitrarily high order in a Taylor series about the chief reference state. This yields both linear (first-order) and nonlinear (higher-order) approximate relative motion solutions in time with the coefficients of the expansion given as functions of the classical osculating chief and deputy orbital elements. The authors show that the second-order time-series solution closely follows the exact unperturbed Keplerian solution, accounting for the higher-order effects of large intersatellite separation. As a verification, the first-order approximation returns the HCW solution parameterized in terms of the classical orbital elements. This method is the same as the absolute difference solution assessed in [28]. In that comparative work, the author presents numerical results that indicate that the absolute difference method is most accurate in modeling relative motion for small along-track angular separations when compared to the quadratic Volterra, double transformation, and approximate double transformation solutions discussed previously.

Another nonlinear mapping equivalent to Eq. (5) is given by Vadali's [74] unit sphere approach, which parameterizes the relative motion in terms of the rotation matrices $\boldsymbol{R}_I^c(\boldsymbol{\alpha}_c)$ and $\boldsymbol{R}_I^d(\boldsymbol{\alpha}_d)$ by considering the relative position projected onto a unit sphere centered on the inertial reference frame origin. Accordingly, the relative position is expressed as a nonlinear function of orbital elements. This formulation is exact for propagation using osculating orbital elements of the chief and deputy, but an average expression for J_2-perturbed motion explicit in time is also derived using the GVE to express the mean rates of change of the classical orbital element angles. A series expansion in eccentricity for the mean radius to be used in scaling the relative motion is also derived to yield a fully time-explicit solution. The dimensional relative position in the RTN frame is then determined by scaling the unit sphere position and velocities for the actual relative position of the spacecraft in time.

It is important to note that the only approximations made in deriving the aforementioned nonlinear mappings is the series truncation for adequately small OED in the case of [73]. No restrictions are placed on the eccentricity of the chief and deputy orbits in either model. Recall that the use of Eq. (3) allows for the exact motion to be more easily determined under any modeled perturbing force via propagation of the orbital element dynamics or a proper application of averaging theory than by seeking a solution to the generally intractable Eq. (1). By then exploiting the previously discussed nonlinear maps, the solution in orbital element state space can be rigorously transformed to a solution in translational state space.

B. Linear Mappings

Linear approximations to the nonlinear expression in Eq. (5) have been widely explored to simplify the ensuing analytical transformations. These first-order simplifications assume small ROE and result in solutions for the relative position and velocity that are linear in the state variables. Using a relative state made up of the quasi-nonsingular OED, Schaub and Alfriend [75] develop a linear mapping to the relative position and velocity state. For an osculating relative state, this offers a closed-form linear approximation to the relative position and velocity as a function of the chief true anomaly, valid for eccentric chief orbits and accurate for when the intersatellite range is small. The same mapping is derived by Alfriend et al. [76] when exploring the loss of modeling accuracy due to linearization, Earth oblateness perturbations, and other effects.

The transformation from a relative state vector comprised of Keplerian OED to the relative position is formulated by Schaub [43], allowing for more geometric insight in orbit design and maneuver planning. Anderson and Schaub [77] later extend this mapping to a fully nonsingular form using the equinoctial OED, following a similar approach as the previous derivations. The more recently derived linear mappings exhibit a similar structure to the early work done by de Vries [39] and Garrison et al. [78], in which different expressions of the linear transformations are derived using alternative OED relative states.

In the framework of the Gim–Alfriend method, the proposed STM captures secular variations of the quasi-nonsingular or fully nonsingular OED due to J_2. Subsequently, a first-order approximation of the Brouwer transformation [48] can be used to map the output to osculating element space by superimposing the short- and long-period element variations. This allows for propagation of the relative osculating state in time instead of using mean elements. It is important to note that the mean-to-osculating transformation derived from Brouwer theory contains a singularity at the critical inclinations, $i \approx 63.4, 116.6$ deg, and thus the STM is not valid near these configurations. The authors find that the singularity becomes a significant issue for model accuracy within ± 0.2 deg of the critical inclinations. Finally, applying the aforementioned linear map from [75] provides a complete propagation of the relative position and velocity state subject to first-order J_2 and arbitrary reference orbit eccentricity.

Early work by D'Amico [79] establishes a mapping between the ROE state containing the relative eccentricity and inclination vectors and the relative position and velocity. In that study, the GVEs are used to express the change in absolute orbital elements as a function of an instantaneous velocity increment. By interpreting the change in absolute orbital elements instead as a set of relative orbital elements and the instantaneous velocity increment instead as a change of initial relative velocity, the GVEs provide a map between the ROE and the relative velocity state. The author then demonstrates a first-order equivalence between the ROE and the integration constants of the HCW solution by comparing the aforementioned GVE-based map with the well-known propagation equations of the HCW model.

In addition to the aforementioned dynamics-based approach, D'Amico and Montenbruck [59] offer an alternative derivation of the same mapping by invoking the assumption of small orbital element differences when applying well-known spherical trigonometry laws to the orbital geometry defined by the orbital elements. A comparison of this geometry-based and the previously mentioned dynamics-based mappings indicates their equivalence. Additionally, it is confirmed by D'Amico [60] that when invoking the near-circular and small ROE assumptions, the transformation developed by Schaub in [43] reduces to a form consistent with the mappings formulated in [59,79] when using the relative eccentricity and inclination vector-based ROE state, with the chief mean argument of latitude replacing the true anomaly as the independent variable of the transformation.

In the development of these mappings, D'Amico clarifies that the HCW solution parameterized in terms of the ROE state demonstrates improved accuracy over the translational state formulation because the relative eccentricity vector retains second-order terms in eccentricity normally dropped in the linearization of the translational state equations of motion. This ROE formulation also removes the erroneous along-track drift present in the traditional rectilinear HCW solution due to poor capturing of the energy matching condition. Accordingly, the equivalent transformations developed in [59,60,79] can be more rigorously interpreted as a map between the ROE state and the curvilinear translational state.

A summary of the surveyed mappings between representations is provided in Appendix B. A brief discussion of the state representations involved as well as the key transformation equations and literature references are provided.

V. Dynamics Models Using Other State Representations

A. State Based on Euler Parameters

Motivated by the singularity introduced in the direction cosine matrix (DCM) mapping from the orbit-fixed perifocal frame to the Earth-centered inertial frame, Gurfil [80] rewrites the solution of the nonlinear two-body problem in terms of Euler parameters. This inherently nonsingular quaternion description is then used to develop a form of the LPE in terms of the Euler parameters that is no longer singular for equatorial and/or circular orbits. The author demonstrates the utility of the new formulation by deriving an averaged set of absolute motion equations subject to J_2. An extension of this methodology to applications in relative motion is developed by Alfriend et al. [6], whereby Gurfil's nonsingular method is used to formulate a relative quaternion describing the orientation of the deputy's RTN frame with respect to the chief's RTN frame. Accordingly, the DCM in Vadali's unit sphere approach, which rotates from the deputy RTN frame to the chief RTN frame, is expressed in terms of the nonsingular relative Euler parameters.

B. State Based on Epicyclic Parameters

Kasdin and Kolemen [81] make use of the Hamiltonian built from the circular, unperturbed relative motion Lagrangian to solve the Hamilton–Jacobi equations for a set of canonical parameters denoted as epicyclic elements. Using the variation of parameters to express the time variation of these epicyclic elements in accordance with Hamilton's equation, the authors obtain a solution to the J_2-perturbed, circular equations of relative motion. Additionally, the authors consider the case of deputy motion relative to a slightly elliptical reference orbit as perturbations to the circular solution, thus prompting a similar approach to combine the J_2 and small eccentricity effects in a closed-form solution. Simulation testing of the J_2-perturbed model with a sun-synchronous circular reference orbit at 1700 km altitude and relative separations as large as 20 km indicate relative position error at approximately 50 m after five orbits. The authors note that the inclusion of slight eccentricity effects in the model was not found to be very effective in higher-eccentricity simulation cases because higher-order corrections are needed to mitigate the sensitivity of J_2-induced relative orbit drift to eccentricity.

C. State Based on Spheroidal Orbital Elements

As an alternative of using Brouwer theory to incorporate the mean effects of nonspherical Earth gravity perturbations, Biria and Russell [82] apply the theory of Vinti, which uses spheroidal coordinates to formulate a gravitational theory that naturally accounts for Earth's oblateness. Modifications to the original Vinti solutions are adopted for application to the relative motion problem and to remove singularities, resulting in a closed-form solution for relative motion expressed as a STM that fully incorporates J_2 and J_3 effects as well as partial J_4 effects. The authors provide compelling evidence to support the claim that applying Vinti's theory results in higher modeling accuracy when compared with Brouwer-based theory because the coordinates naturally model a spheroidal planet. Brouwer theory instead relies on perturbation methods to address Earth oblateness effects not included in the spherical reference model. Moreover, the Vinti-based model eliminates the motion prediction singularities at the critical inclination, which cause problems for Brouwer-based propagation methods like those discussed in [47].

A tabulated summary of the surveyed dynamics models is provided in Appendix A. Models are summarized according to state representation, orbit regime, and perturbations included. The relevant references cited in the body of this paper are provided with each table entry.

VI. Comparative Assessment

To provide a meaningful comparison of several surveyed dynamics models, the following architecture is structured to provide a consistent, repeatable, and rigorous assessment via high-fidelity simulation. A designated C++ software library is developed for implementing the dynamics models in conjunction with a high-fidelity numerical orbit propagator serving as the simulated truth. The models are tested using consistent initial conditions on the reference orbit and relative motion for a variety of test scenarios designed to highlight the relative strengths and weaknesses of the chosen dynamics models. Finally, a detailed error analysis is carried out that provides a one-to-one comparison of the modeling performance against the numerically propagated truth simulation.

A. Subset of Relative Motion Dynamics Models

Although the survey provides a broad sampling of the existing relative dynamics models available in the literature, a comparative assessment that includes the entire set of dynamics models is neither pragmatic nor necessary. Instead, a subset of the surveyed models is chosen to represent a comprehensive state of the art in closed-form solutions across several state representations, with different limitations on chief eccentricity, linearization assumptions, and perturbations included. The models considered in the comparison are the curvilinear HCW [13] model, the quadratic Volterra model [28], the Schweighart–Sedwick model [18], the Yamanaka–Ankersen STM [34], the Broucke STM [38], the Gim–Alfriend STM [47,49], the GAM STM [63], the KGD STM [52], the Yan–Alfriend nonlinear theory [53,54], and the Biria–Russell Vinti method [82]. Figure 1 graphically represents a broad classification of each selected model by its state representation and the assumptions used in deriving the closed-form solution.

Regarding the Schweighart–Sedwick method, the original formulation restricts the initial conditions to remove any constant offset or secular drift terms in the solution, and the authors acknowledge that the model formulation does a poor job at predicting in-track drift. The model is also derived assuming that the chief spacecraft is initialized at the equator. Furthermore, the original initialization procedure specifies a reference orbit and relative state initial condition, and from this they derive the motion of the chief and deputy in time. The structure of this comparative assessment instead proceeds from specified chief and deputy initial conditions and propagates the motion using the analytical solution. To accommodate this, the equations of motion were first resolved to allow for arbitrary relative initial conditions without restricting the offset and secular drift terms to be zero. Then, the model is initialized assuming that, at

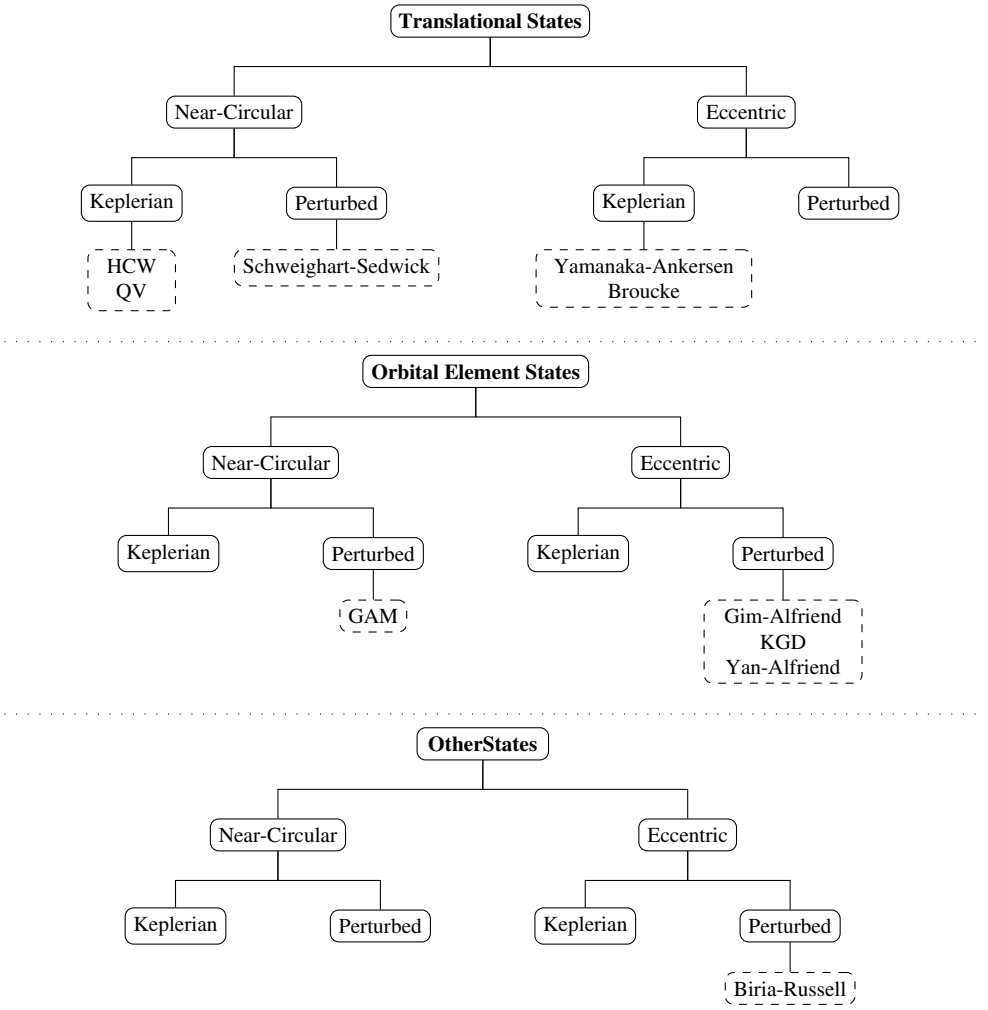

Fig. 1 Categorization of closed-form dynamics models included in the comparison.

the initial time, the chief is lying on the circular reference orbit about which the equations are linearized. It is worth noting that, in both the original formulation and our correction, if the given chief initial velocity causes it to drift from this reference orbit, the linear equations of motion quickly become invalid, and performance suffers.

It is also important to mention a distinction made in the comparative assessment with respect to the Gim–Alfriend STM implementation. The core STM of the Gim–Alfriend method uses either mean singular OED or mean nonsingular equinoctial OED as the relative state parameterization, whereas the full Gim–Alfriend STM superimposes linearized transformations between curvilinear coordinates and the core OED to propagate the curvilinear relative motion from the core STM. To isolate the effects of these linearized coordinate transformations, the comparative assessment includes two separate implementations of the Gim–Alfriend STM. In the first, the full STM is used to linearly propagate a curvilinear relative initial condition to the curvilinear relative state at a final time subject to J_2. The second implementation employs only the core mean OED relative state propagation; the full nonlinear Brouwer mean-osculating and orbital element to translational state transformations are used in initializing and to transform from mean OED relative state to the desired state space for error analysis. A more detailed description of the state transformations required for model initialization and output mapping is given in the next section.

Finally, although both the KGD and GAM STMs include the effects of time-varying differential drag and secular J_2 perturbations, the comparative assessment only implements the solutions pertaining to J_2-perturbed relative motion. This is largely due to the fact that effective drag modeling in these two models requires estimating several parameters (e.g., the time derivative of the relative semimajor axis and the time derivatives of the relative eccentricity vector components). Thus, uncertainty in these estimates results in substantial modeling error. Simply assuming perfect knowledge of these parameters for the sake of this comparative assessment is unrealistic and inconsistent. The comparative work of Alfriend and Yan [3] also notes the difficulties in quantifying atmospheric drag modeling performance and does not include any studies of differential drag effects on relative motion.

B. Software Implementation

This section details the model and simulation implementations and the structure of the comparative assessment testing environment. Each model is written as a C++ S-function, precompiled for integration within MATLAB/Simulink. The reason for this is to support fair timing comparisons between models as well as between the reference numerical integration. Furthermore, implementing the comparative assessment in Simulink provides a framework that is flexible and agile enough to incorporate different test scenarios quickly.

The two selections to be made in specifying initial conditions for a simulation are the chief absolute state and the relative state defining the motion of the deputy with respect to the chief. In turn, this corresponds to a unique chief and deputy initial state for each test case. The initial conditions for the absolute chief orbit are given in terms of mean Keplerian orbital elements. As in previous sections, this chief state vector is denoted by $\boldsymbol{\alpha}_c$. To specify the initial conditions of the deputy with respect to the chief, a relative state of the mean quasi-nonsingular ROE that includes the relative eccentricity and inclination vectors $\delta\boldsymbol{e}$ and $\delta\boldsymbol{i}$ is used. This relative state is defined as the following combination of absolute mean orbital elements

$$\delta\boldsymbol{\alpha} = \begin{pmatrix} \delta a \\ \delta\lambda \\ \delta e_x \\ \delta e_y \\ \delta i_x \\ \delta i_y \end{pmatrix} = \begin{pmatrix} (a_d - a_c)/a_c \\ (u_d - u_c) + (\Omega_d - \Omega_c)\cos i_c \\ e_d \cos\omega_d - e_c \cos\omega_c \\ e_d \sin\omega_d - e_c \sin\omega_c \\ i_d - i_c \\ (\Omega_d - \Omega_c)\sin i_c \end{pmatrix} \tag{7}$$

where a, e, i, Ω, and ω are the classic mean Keplerian orbital elements, and $u = M + \omega$ is the mean argument of latitude written in terms of the mean anomaly M.

The reference truth for each test is computed by a numerical integration of the absolute equations of motion of the chief and deputy in Earth-centered-inertial (ECI) coordinates, subject to a specified force model. The truth ECI states are converted exactly to a truth relative state described in the rectilinear coordinates of the chief RTN frame. To initialize the truth numerical integration, $\boldsymbol{\alpha}_d$ is computed from $\delta\boldsymbol{\alpha}$ and $\boldsymbol{\alpha}_c$, and the two absolute sets of mean elements are converted to their osculating counterparts, $\tilde{\boldsymbol{\alpha}}_c$ and $\tilde{\boldsymbol{\alpha}}_d$. Note that, from now on, $\tilde{(\cdot)}$ explicitly denotes an osculating element set. The mean-to-osculating transformation is nonlinear in the orbital elements but introduces errors of $\mathcal{O}(J_2^2)$ due to linearizing (with respect to J_2) the generating functions used to superimpose short- and long-period oscillations on the mean element set. Finally, the osculating elements are used to compute the initial ECI position and velocity of the chief and deputy through the nonlinear functions $\boldsymbol{r}(\tilde{\boldsymbol{\alpha}})$ and $\boldsymbol{v}(\tilde{\boldsymbol{\alpha}})$ introduced in the context of Eq. (5). The initialization of the numerical integration is graphically depicted in the top row of Fig. 2.

Because the assessment models operate with different state parameters (i.e., relative rectilinear and curvilinear translational elements, mean OED, mean relative eccentricity/inclination-based quasi-nonsingular ROE, or absolute ECI chief and deputy states), care must be taken to ensure correct transformations from the initial chief and initial quasi-nonsingular ROE state to proper initial conditions in the model-specific state. To initialize each analytical relative motion model, the osculating reference initial conditions are converted nonlinearly to the corresponding state space of each model. In the center row of Fig. 2, the osculating chief and deputy ECI states are converted exactly to the rectilinear and curvilinear chief RTN frame coordinates for analytic propagation based in the translational state space. The bottom row of Fig. 2 demonstrates the conversion from the initial chief mean orbital elements and initial mean quasi-nonsingular ROE to initial mean OED. Accordingly, all necessary transformations from the specified initial $\delta\boldsymbol{\alpha}$ and $\boldsymbol{\alpha}_c$ states to the model-specific states have been established.

The outputs of each analytic propagation and the numerical integration span many state spaces and must be rectified to a single space for error analysis. Outputs in the model-specific state are transformed nonlinearly to the relative rectilinear position and velocity in the chief RTN frame. This allows for direct comparison of the analytically propagated states with the truth model for each test case. Figure 3 shows the process of transforming the model-specific states to chief RTN frame components. The dashed lines in the bottom row abbreviate the conversion process from mean absolute states to osculating relative position and velocity, detailed in the row above.

It is important to note that, in the analytic propagation of each relative motion model, there is a dependence on knowledge of the chief absolute state. To be consistent across all models, the chief state is propagated for each approximate model according to the assumptions of that model. That is, if the analytic solution is developed assuming a two-body gravitational field, the chief orbital elements, with exception of the mean anomaly, remain constant. Alternatively, the mean chief elements are updated according to the mean angle rates due to J_2 for a model that includes the secular effects of J_2 on the relative motion. Though important to be consistent, the error introduced by an imperfect representation of the chief state is negligible compared to the error due to the approximations made to obtain closed-form solutions to the relative dynamics.

C. Evaluating Model Performance

With the subset of dynamics models chosen and the simulation validation architecture established, the methodology for evaluating model performance is now introduced. First, the discussion begins with the choice of initial conditions on the chief absolute orbit and on the relative orbit, followed by a brief description of the three force

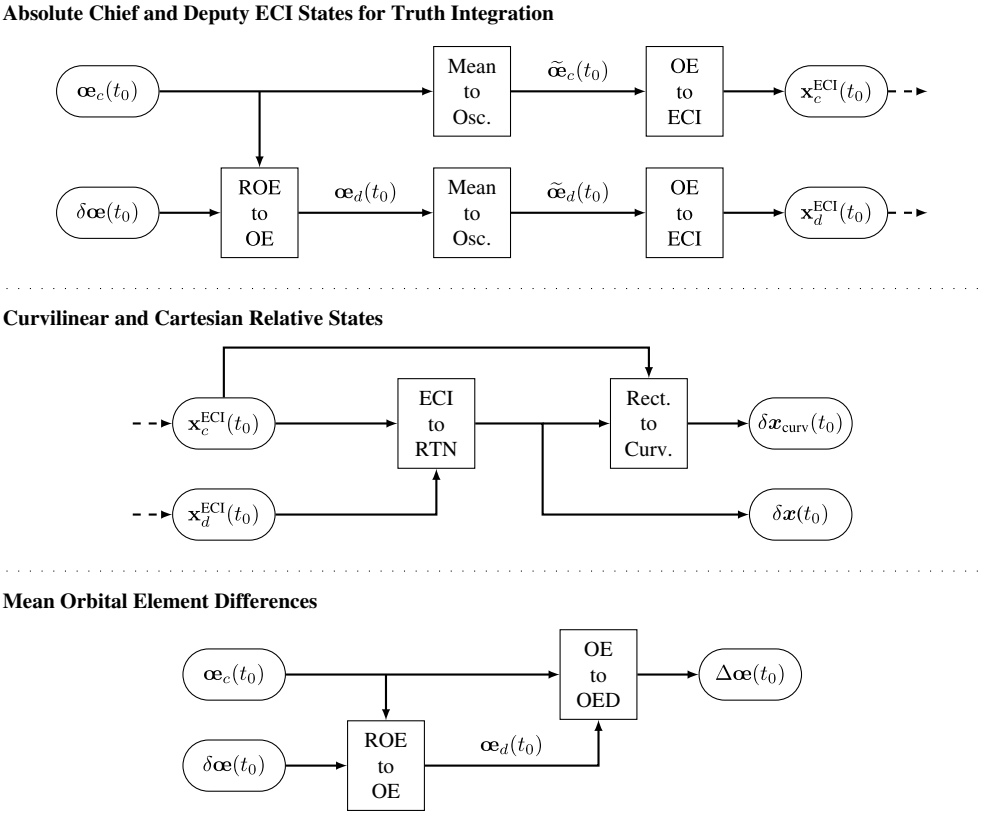

Fig. 2 State transformations for initializing reference (top) and analytic model propagations.

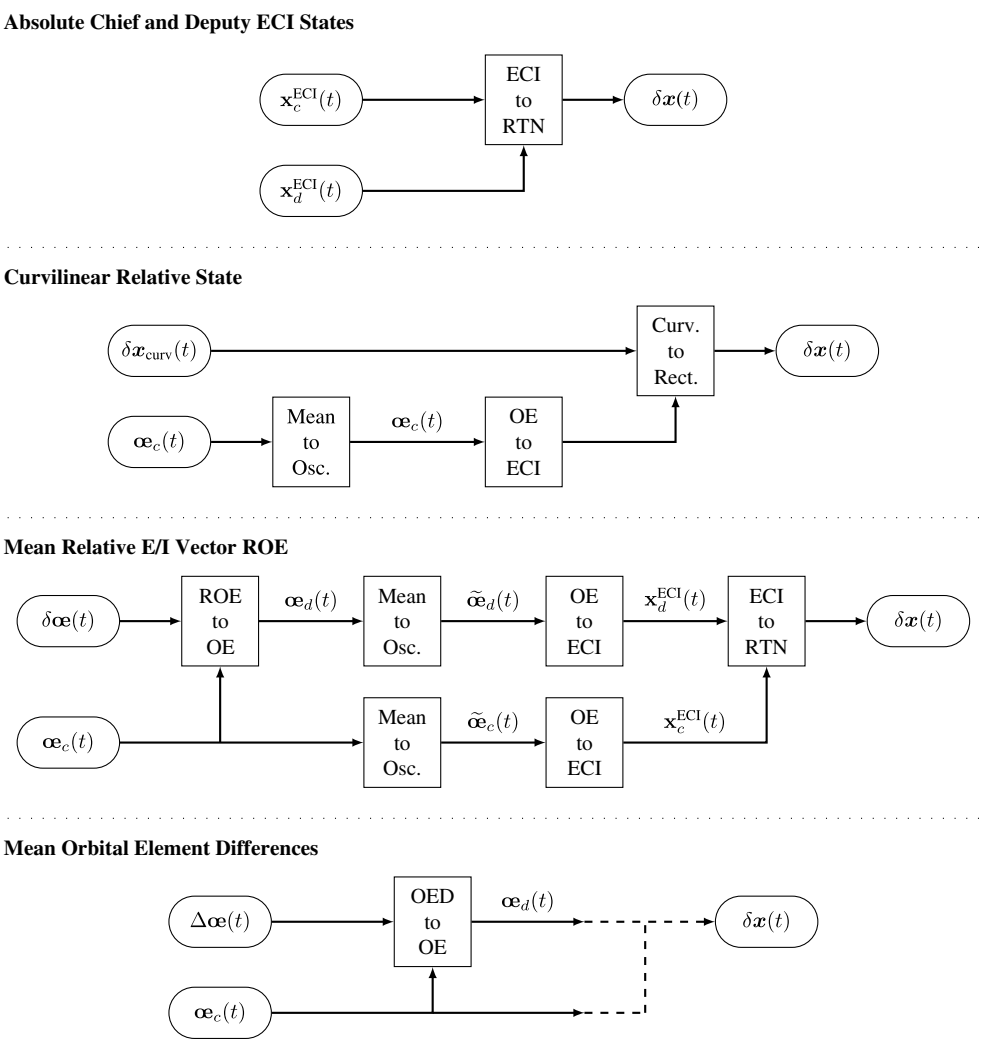

Fig. 3 Output state transformations for error comparison in Hill's frame Cartesian coordinates.

models used to validate and compare the analytical models. The test procedures are designed to evaluate the model performance as a free parameter of interest (e.g., the chief eccentricity or the interspacecraft separation) is varied about the nominal configurations. Finally, model performance metrics and error analysis methods are outlined.

1. Initial Conditions and Test Scenarios

As described previously, the initial conditions for the absolute chief orbit are given in terms of the mean Keplerian orbital elements at the start of the simulation. Two nominal chief orbits are considered as a starting point about which to vary parameters. The first is a near-circular sun-synchronous LEO with eccentricity of 0.001 and a 750 km altitude, common to many Earth imaging missions and notably the PRISMA formation flying mission [83]. To capture an eccentric reference orbit, the second chief orbit is a modification of the first nominal configuration to an eccentricity of 0.5 and a 750 km perigee altitude.

To specify the relative motion, the mean quasi-nonsingular ROE state [see Eq. (7)] is now quantified. First, the relative motion test cases are constrained to be bounded and centered, thus fixing the first two elements of the relative state vector δa and $\delta\lambda$ to zero. With zero relative semimajor axis (i.e., $\delta a = 0$), Keplerian orbit effects that cause a drift in the relative separation due to differences in the spacecraft mean motions are not present. Although a mean along-track separation created by nonzero $\delta\lambda$ could also be used to vary the average spacecraft separation, to restrict the amount of free parameters, it is fixed to zero so that separation is only a function of the relative eccentricity and inclination vectors.

To again reduce the number of free parameters being considered, a choice is made to constrain the magnitudes and orientations of the relative eccentricity and inclination vectors to be equal. In this case, the relative motion for near-circular orbits transcribes the familiar 2×1 ellipse in the radial/along-track plane and circular motion in the radial/cross-track plane. Accordingly, a single parameter (the norm of $\delta\boldsymbol{e}$ or $\delta\boldsymbol{i}$) defines the average spacecraft separation. The minimum and maximum separations are straightforward to compute as $a_c\|\delta\boldsymbol{e}\|$ and $\sqrt{5}a_c\|\delta\boldsymbol{e}\|$, respectively, for a near-circular chief. It is reasonably assumed that these geometric implications hold approximately in the eccentric orbit test cases.

The final free parameter to constrain is the orientations of the relative eccentricity and inclination vectors, which have already been chosen to be equal. Because the J_2 perturbation causes a secular shift of the orbital planes (δi_y drifting) due to a difference in inclination (i.e., δi_x nonzero), the y components of the relative eccentricity vector and inclination vectors are set to zero. Accordingly, the relative separation is defined only by the x-component magnitudes (which have already been constrained to be equal). This choice results in a worst-case performance for any model that does not include the effects of J_2 because the aforementioned drift will go completely unmodeled.

Three test scenarios are specified in which a given free parameter is varied while holding all others constant at the nominal configuration. Table 1 specifies the absolute and relative orbit initial conditions for each of the three scenarios. Note that scenario 1 is designed to test the relative motion model performance as a function of chief orbit eccentricity, which is varied from 10^{-4} to 0.7 (denoted in the table as

Table 1 Absolute and relative initial conditions for the three test scenarios

	Chief orbit, $\boldsymbol{\alpha}_c(t_0)$						Relative orbit, $\delta\boldsymbol{\alpha}(t_0)$					
Number	$h_{p,c}$, km	e_c	i_c, deg	Ω_c, deg	ω_c, deg	M_c, deg	$a_c\delta a$, m	$a_c\delta\lambda$, m	$a_c\delta e_x$, m	$a_c\delta e_y$, m	$a_c\delta i_x$, m	$a_c\delta i_y$, m
1	750	$[10^{-4}:0.7]$	98.2	30	0	0	0	0	100	0	100	0
2	750	0.001	98.2	30	0	0	0	0	$[1:10^5]$	0	$[1:10^5]$	0
3	750	0.5	98.2	30	0	0	0	0	$[1:10^5]$	0	$[1:10^5]$	0

$[10^{-4}:0.7]$), while maintaining a fixed short-range relative geometry with maximum separation on the order of a few hundred meters. Instead, scenarios 2 and 3 vary the interspacecraft separation by varying the relative eccentricity and inclination vector magnitudes from 1 to 10^5m for the nominal near-circular and eccentric chief orbits (denoted in the table as $[1:10^5]$). By varying the separation, these scenarios will reveal the operating geometries for which models that assume linearized relative motion can be reasonably applied. For scenarios 2 and 3, separations range from approximately 2 m to 250 km to capture a broad operational envelope.

The selection of a truth model is the final component needed to fully specify the conditions for each simulation. In general, there is the option of comparing against a mathematical truth or a physical truth. Here, the mathematical truth is defined as a reference simulation subject to the assumptions and constraints imposed in the development of a closed-form model. A physical truth, on the other hand, is the simulation that models most closely the true dynamical environment in the highest fidelity available. The objective of this study is to examine the performance of models outside of their derived range of validity; thus, three representative models are selected. For the first model, a numerical integration of the absolute equations of motion of both spacecraft subject to an unperturbed spherical Earth gravity field is used to test each analytical model's propagation of Keplerian relative motion. The second model is a numerical integration including conservative perturbation forces due to the J_2 through J_5 zonal gravity coefficients. This model is used for validation in multiple research studies (see [47,82]) and so is retained in this assessment for consistency with previous works. Finally, the third model is derived from a numerical integration including a full high-fidelity perturbation environment, complete with a 120×120 GRACE gravity field, third-body sun and moon forces, solar radiation pressure (SRP), atmospheric drag using a Harris–Priester density model, and relativistic and tidal effects. The spacecraft properties for the high-fidelity force model are replicated from the PRISMA mission and reproduced in Table 2 and found in [60]. Table 3 summarizes the chosen force models. In each case, the numerical integration of the absolute equations of motion for each spacecraft in ECI coordinates is performed, and the outputs are transformed to the relative rectilinear state in the chief RTN frame.

Table 2 Chief and deputy spacecraft properties for high-fidelity simulation

Property	Chief	Deputy
Mass, kg	154.4	42.5
Drag area, m^2	1.3	0.38
SRP area, m^2	2.5	0.55
Drag coefficient C_D	2.5	2.25
SRP coefficient C_r	1.32	1.2

Table 3 Reference numerical propagation force models

Model number	Force model
1	Spherical Earth gravity (unperturbed Keplerian motion)
2	5×0 gravity field
3	120×120 gravity field, atmospheric drag, SRP, third-body sun and moon, relativistic and tidal effects

2. Performance Metrics and Error Analysis

An error metric for linear dynamics models is developed by Junkins et al. [84], and in [3], it is used as inspiration for a modeling error index that is applicable to both linear and nonlinear relative motion dynamics models. The modeling error index is defined as a measure of the maximum error of an analytically propagated relative trajectory over a fixed timespan, normalized by the size of the relative motion. For a scalar state, it is proportional to the percentage error. However, for useful insight into the model performance, it is often relevant to consider an absolute error metric (i.e., in meters of error) and to capture errors in both the position and velocity components. Therefore, for this comparative assessment, a modified modeling error metric is proposed. The metric is defined as the maximum 2-norm of the relative state error over a fixed simulation time:

$$\nu = \max_i \|\boldsymbol{W}(\boldsymbol{\delta x}(t_i) - \boldsymbol{\delta x}_{\text{ref}}(t_i))\|_2, \quad \text{for } t_i \in [t_0, t_f] \tag{8}$$

where $\boldsymbol{\delta x}(t_i)$ is the relative state computed by rigorously transforming the output from the propagated model-specific coordinates to the rectilinear relative state in the chief RTN frame (see Fig. 3), and $\boldsymbol{\delta x}_{\text{ref}}$ is the truth relative state in the same coordinates. The weighting matrix $\boldsymbol{W} = \text{diag}(1, 1, 1, n_c^{-1}, n_c^{-1}, n_c^{-1})$ provides a useful depiction of maximum state error with dimensions of length by nondimensionalizing time in the relative velocity using the chief mean motion n_c.

D. Numerical Results

The three scenarios of Table 1 are evaluated against the three force models of Table 3, resulting in nine total performance tests for each of the selected relative dynamics models. The error metric [see Eq. (8)] and propagation runtime are obtained over a 24 h simulation period for each test case. The numerical results are summarized in this section. Note that, as implemented, the Biria–Russell model contains a singularity if $J_2 = 0$. Accordingly, it is not included in the comparisons against a Keplerian force model.

1. Scenario 1

First, the simulation results for scenario 1 are presented. Recall that this scenario is defined by fixed relative motion geometry with small separation (~300 m) and a chief orbit with eccentricity varied over the range 10^{-4} to 0.7. Figures 4–6 depict the modeling error metric trends over the varied chief eccentricity parameter for the three reference force models, respectively.

When compared against a Keplerian reference (Fig. 4), it is immediately clear that the orbital element-based models perform better across the entire chief eccentricity spectrum than models that propagate translational states. This is largely because, for unperturbed orbits, the orbital elements (with the exception of the mean/true anomaly) remain constant. The effect of linearization is thus confined to errors in the time evolution of these anomaly elements. Recall that, although the Gim–Alfriend core STM is formulated in terms of the true anomaly, the KGD and GAM STMs are developed using the mean anomaly. For unperturbed orbits of equal energy (i.e., $\delta a = 0$), the mean anomaly difference ΔM is constant irrespective of eccentricity, whereas the difference in true anomaly Δf generally grows. Accordingly, the Gim–Alfriend core STM performs approximately three orders of magnitude worse than the GAM and KGD STMs due to the linearization of the Δf evolution. Finally, the Yan–Alfriend nonlinear method does not yield significant improvements over the GAM and KGD STMs because the interspacecraft separation is small for scenario 1.

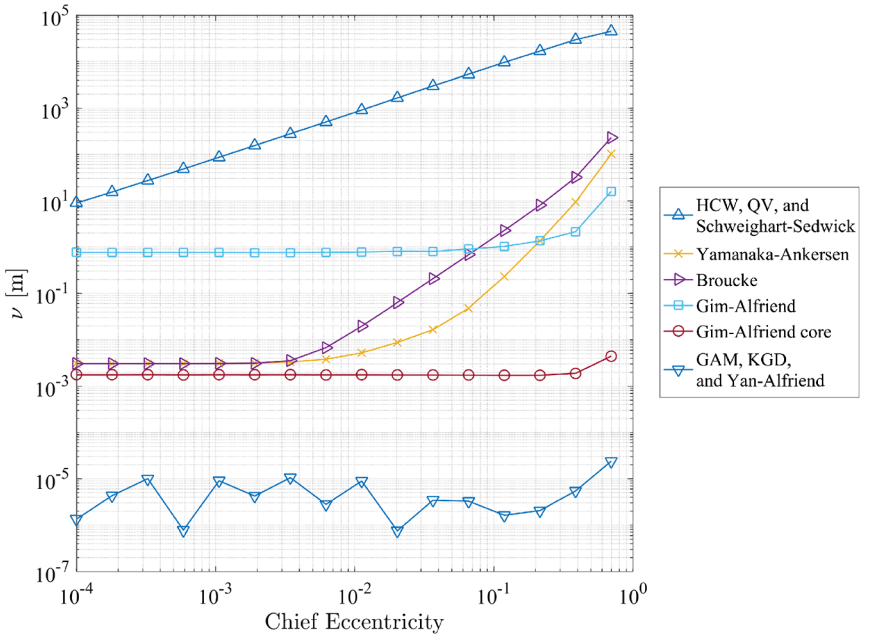

Fig. 4 Scenario 1 modeling error compared with Keplerian truth.

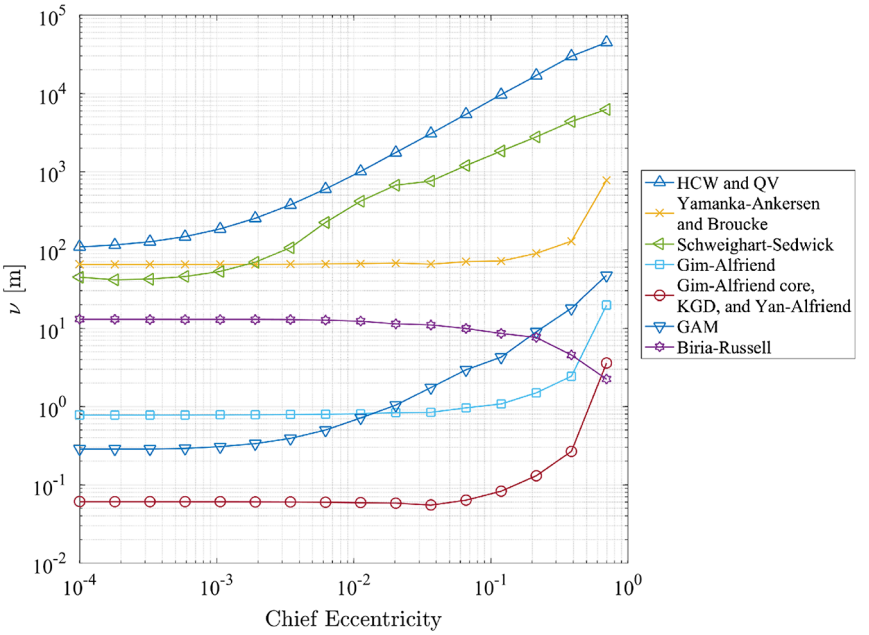

Fig. 5 Scenario 1 modeling error compared with J_2–J_5 truth.

As expected, the HCW, quadratic Volterra, and Schweighart–Sedwick models perform the worst across the board because they do not account for chief orbit eccentricity. The nonlinear effects captured in the quadratic Volterra method do not provide improved performance over the curvilinear HCW and Schweighart–Sedwick models because interspacecraft separation is generally small. Both the Broucke and Yamanaka–Ankersen STMs yield similar accuracy as the core Gim–Alfriend STM up to a chief eccentricity of 0.01. From there, the propagation accuracy of the Yamanaka–Ankersen and Broucke models steadily worsens over the remainder of chief eccentricity values. The most likely cause of this performance degradation is due to the fact that, as chief orbit eccentricity increases, the relative separation fluctuates more drastically while the chief is near perigee. Accordingly, the linearization assumption of small interspacecraft separation with respect to the chief absolute radius (which is smallest at perigee) breaks down, and neglected higher-order terms become significant error sources. Finally, as compared with the modeling performance of its core counterpart, the full Gim–Alfriend STM results in three orders of magnitude of additional error brought about by using linearized coordinate transformations between curvilinear elements and OED. It is important to reiterate that the core Gim–Alfriend STM implementation is followed by nonlinear transformations from mean to osculating orbital elements and from osculating orbital elements to the rectilinear relative position and velocity components for error analysis; instead, the full Gim–Alfriend STM includes first-order coordinate transformations from mean to osculating orbital elements and from osculating orbital elements to curvilinear coordinates.

Looking now to the scenario 1 model evaluation against the higher-order gravity force model (Fig. 5), several key features are noteworthy. First, the Yan–Alfriend, Gim–Alfriend core, and KGD models all perform very similar over the entire range of chief eccentricity values. This indicates that, even though the Yan–Alfriend method effectively includes $\mathcal{O}(J_2^2)$ terms (which are on the same order as J_3 terms), these effects offer minimal performance improvement over including only secular J_2 terms. The GAM STM

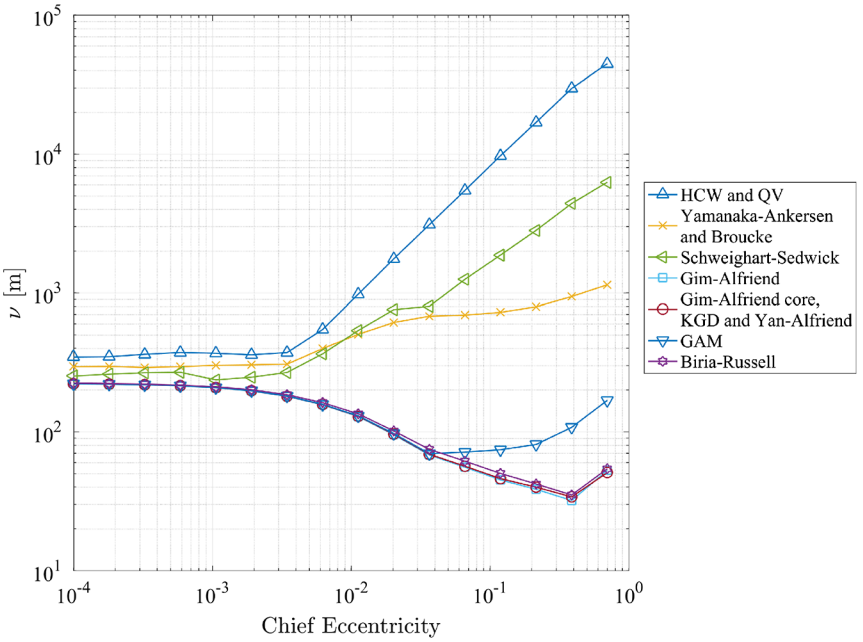

Fig. 6 Scenario 1 modeling error compared with full-force truth.

results in errors on the same order magnitude as the Yan–Alfriend, Gim–Alfriend core, and KGD models for chief eccentricity as large as 0.01. Past that value, the solution suffers large error increases due to unmodeled chief eccentricity effects. Similar to the Keplerian force model results in Fig. 4, the full Gim–Alfriend STM results in modeling error that is approximately one order of magnitude larger than the core STM propagation for all chief eccentricities. As expected, the Biria–Russell model performs with comparable accuracy to the full Gim–Alfriend solution, with a slight improvement as orbit eccentricity increases.

The Broucke and Yamanaka–Ankersen methods perform very similarly to one another but suffer errors that are orders of magnitude larger than the other solutions discussed thus far due to assuming unperturbed orbits. Instead, at small chief eccentricities, the Schweighart–Sedwick model outperforms the Broucke and Yamanaka–Ankersen methods because it incorporates first-order effects of J_2. However, by comparing the performance trends of the Yamanaka–Ankersen, Broucke, and Schweighart–Sedwick models at larger eccentricities, it is clear that the effect of unmodeled chief eccentricity as low as $e_c = 0.01$ is more detrimental than the effect of unmodeled J_2 perturbations. Finally, as expected the HCW and quadratic Volterra models perform the poorest over the entire swath of chief eccentricity values because they assume a circular, unperturbed reference orbit.

The comparative results for scenario 1 subject to evaluation against a full-force truth model are shown in Fig. 6. First, it is immediately clear that the Yan–Alfriend, KGD, Gim–Alfriend (full and core), and Biria–Russell models all perform very similarly over the chief eccentricity spectrum. This is largely because any performance differences between these solutions (see for example the differences shown in Fig. 5) are small compared to the overall error introduced from each neglecting the multitude of additional perturbations included in the full-force truth model. Furthermore, as chief eccentricity increases, these five solutions show a distinct decrease in error because more time is spent in higher altitudes where the effects of unmodeled high-order gravity and drag are largely negligible. Instead, solar radiation pressure and third-body perturbations become more relevant but result in differential accelerations that are orders of magnitude smaller than those in near-circular orbits. The modeling accuracy trends of the GAM model are comparable to the previously mentioned solutions up until neglected chief eccentricity effects become relevant around $e_c = 0.05$.

Similar to the results of Fig. 5, the Schweighart–Sedwick model outperforms the Broucke and Yamanaka–Ankersen solutions at small eccentricities but comparatively worsens at larger eccentricities. Again, it stands to reason that, for orbit eccentricity larger than 0.05, it is more beneficial to use a model that does not assume a circular reference orbit over a model that includes first-order J_2 effects but does assume a circular reference orbit. Finally, as expected, the HCW and quadratic Volterra methods perform the worst because they do not account for chief orbit eccentricity nor any perturbations. Furthermore, at such small separations (hundreds of meters), the quadratic Volterra solution does not provide any distinguishable benefits over the curvilinear HCW implementation.

2. *Scenario 2*

Scenario 2 consists of a chief spacecraft in a near-circular sun-synchronous LEO with perigee altitude of 750 km and a nominally bounded and centered relative motion trajectory (see Table 1). For this set of assessments, the interspacecraft separation is varied from approximately 2 m to 250 km. Figures 7–9 depict the modeling error metric trends over the varied separation for each of the three force models.

As before, the discussion begins first with the results from evaluating models against a Keplerian force model (Fig. 7). The benefits of formulating solutions using the mean anomaly is immediately evident from the very small modeling error demonstrated by the KGD and GAM STMs. Recall that, for $\delta a = 0$, the difference in mean anomaly ΔM is constant, whereas the difference in true anomaly Δf varies with time. Accordingly, linear relative motion models formulated in terms of the true anomaly must approximate the time-evolution of Δf by truncating higher-order terms in separation. The persistently increasing propagation error shown by the core Gim–Alfriend STM is a direct result of this linearization. A similar linearization effect is present in the respective state spaces of the Broucke, Yamanaka–Ankersen, Schweighart–Sedwick, and HCW models, as indicated by propagation errors that increase as interspacecraft separation increases. Instead, notice that the Yan–Alfriend nonlinear method (which retains second-order terms in the ROE) propagates at comparable accuracy to KGD and GAM, and the quadratic Volterra solution (which includes second-order terms in the translational state variables) outperforms the HCW model by a factor of 10 at large separation.

The inclusion of gravitational perturbations in the truth model results in several noteworthy features shown in Fig. 8. First, although the Yan–Alfriend, KGD, GAM, and Gim–Alfriend models all result in comparable propagation accuracy for smaller interspacecraft separations, the Yan–Alfriend outperforms the others at large

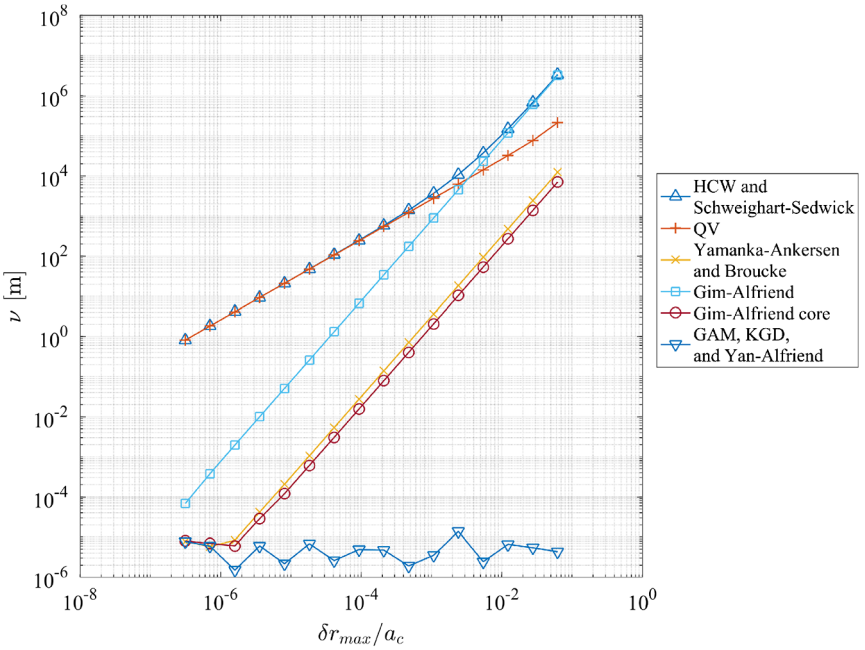

Fig. 7 Scenario 2 modeling error compared with Keplerian truth.

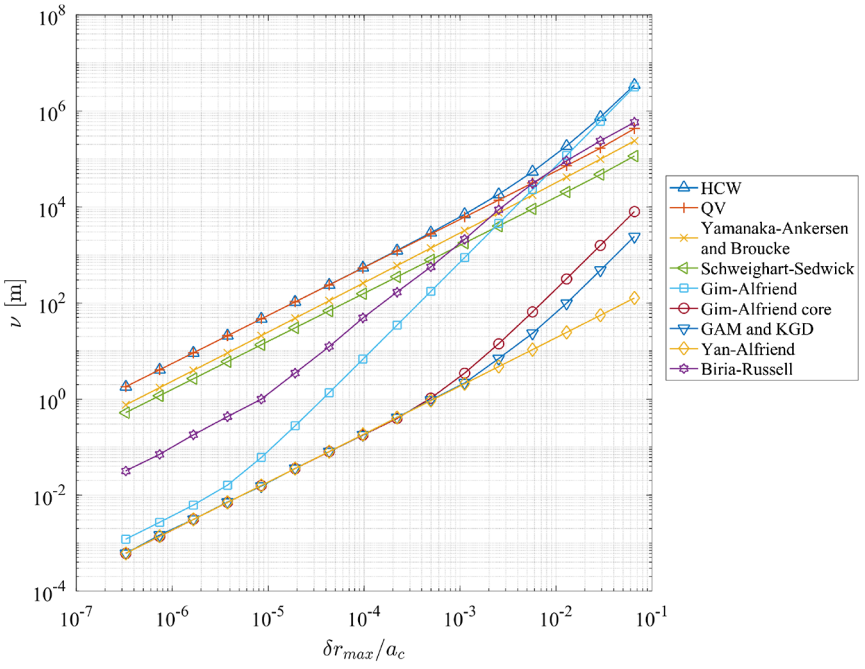

Fig. 8 Scenario 2 modeling error compared with J_2–J_5 truth.

separations by retaining second-order terms. Similarly, the GAM and KGD STMs outperform the Gim–Alfriend core STM as separations become larger due to the aforementioned benefits of formulating the models in terms of the mean anomaly instead of the true anomaly. The Biria–Russell and full Gim–Alfriend models result in similar capabilities, with the Gim–Alfriend STM showing comparatively more accuracy at smaller separations and the Biria–Russell model outperforming at larger separations. Note that the full Gim–Alfriend STM error approaches similar magnitude as the curvilinear HCW implementation for very large separations. This is largely due to the linearized coordinate transformation from orbital element space to curvilinear space.

Because scenario 2 defines a near-circular chief orbit, the Schweighart–Sedwick model is able to provide an provide an improvement in propagation accuracy over the Broucke, Yamanaka–Ankersen, HCW, and quadratic Volterra solutions for all simulated interspacecraft separations by including J_2 perturbation effects. Finally, the second-order terms retained in the quadratic Volterra method result in modeling accuracy that is approximately 10 times better than the curvilinear HCW solution.

The same general trends described in the context of Fig. 8 are present in the results in Fig. 9 obtained by evaluating the models against a full-force truth propagator. There are, however, a few noteworthy distinctions to be made. First, there is a distinguishable region of separations ($\delta r_{\max}/a_c \leq 0.005$) where the modeling errors of the Yan–Alfriend, KGD, GAM, and Gim–Alfriend core solutions remain relatively constant. This strongly indicates that these four models have a larger range of applicability before the errors due to solution truncation dominate. Instead, the propagation accuracy of the remaining models degrade rather sharply as separation increases due to the combined effect of linearization error and unmodeled perturbations.

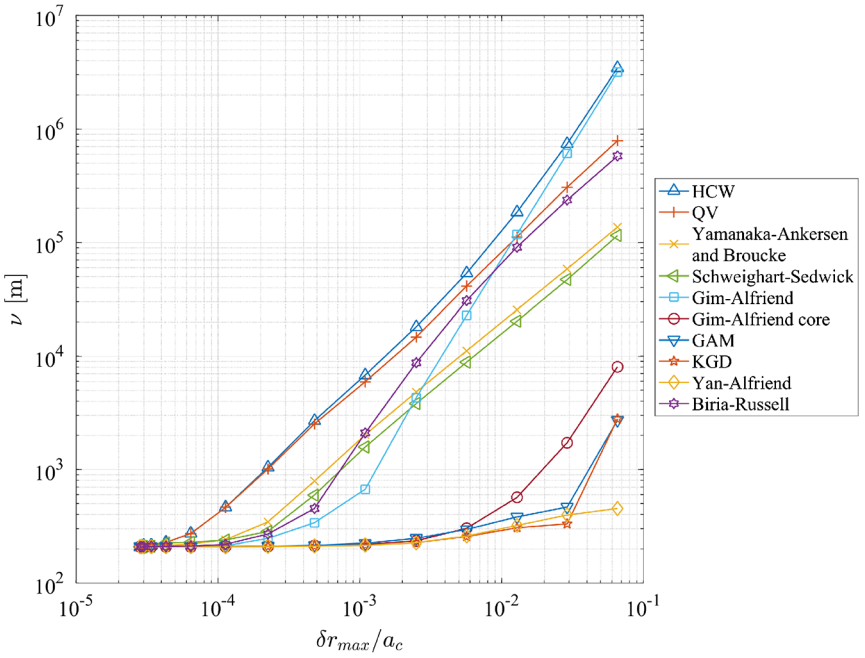

Fig. 9 Scenario 2 modeling error compared with full-force truth.

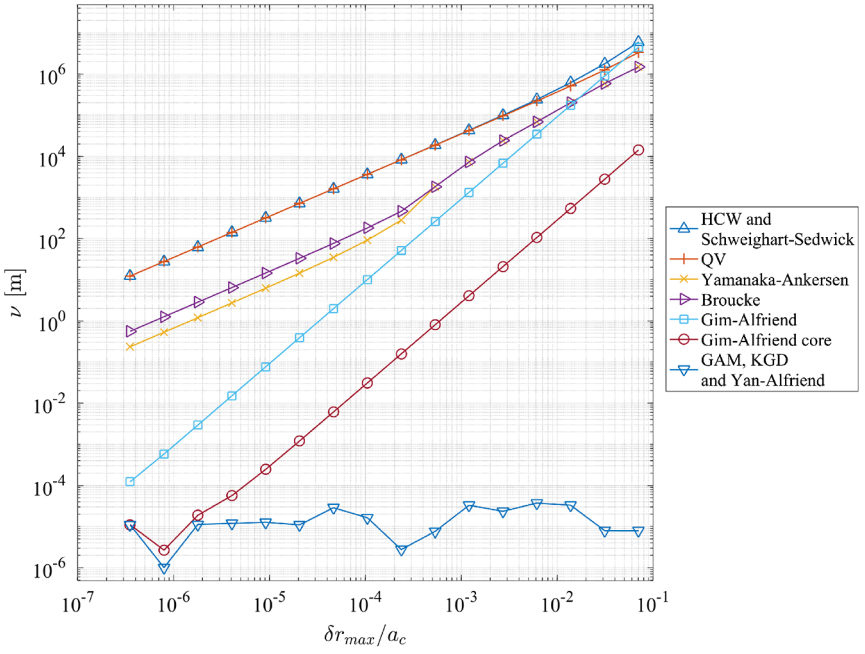

Fig. 10 Scenario 3 modeling error compared with Keplerian truth.

3. *Scenario 3*

Finally, the results for scenario 3 are presented in Figs. 10–12. This scenario defines a highly inclined, eccentric chief orbit with $e_c = 0.5$ and a perigee altitude of 750 km (see Table 1). The relative separation is varied just as in scenario 2. In general, the results for scenario 3 follow comparable trends to those of scenario 2. Accordingly, the following discussions highlight distinct performance features that are different between the scenario sets.

Looking first at the performance against a Keplerian force model as shown in Fig. 10, there are a few noteworthy performance trends to mention. First, as compared with their performance in Fig. 7, the Broucke and Yamanaka–Ankersen solutions propagate with several orders of magnitude more error. The root cause for the additional error can be attributed to the same linearization effects discussed in the context of Fig. 4, where it was hypothesized that the truncation of higher-order solution terms is more detrimental in eccentric orbit where the separation is varying largely during certain phases of the orbit. Finally, the benefits of retaining nonlinear terms in the quadratic Volterra method are largely surpassed by the errors due to assuming a circular reference orbit. Accordingly, the performance of the quadratic Volterra solution is much more comparable to that of the HCW and Schweighart–Sedwick models at large separations in scenario 3 than it was in scenario 2.

The model performances versus a perturbed force model (Figs. 11 and 12, respectively) share several similar trends. Just as in scenario 2, the Yan–Alfriend, KGD, and Gim–Alfriend core solutions all perform with relatively constant accuracy in the region $\delta r_{\max}/a_c \leq 0.001$. Now, however, the GAM STM generally performs worse due to assuming a circular chief orbit, whereas the Biria–Russell solution improves substantially because the Vinti model tends to propagate more accurately at larger eccentricities. This is consistent with the results of Fig. 5. Finally, the advantage of

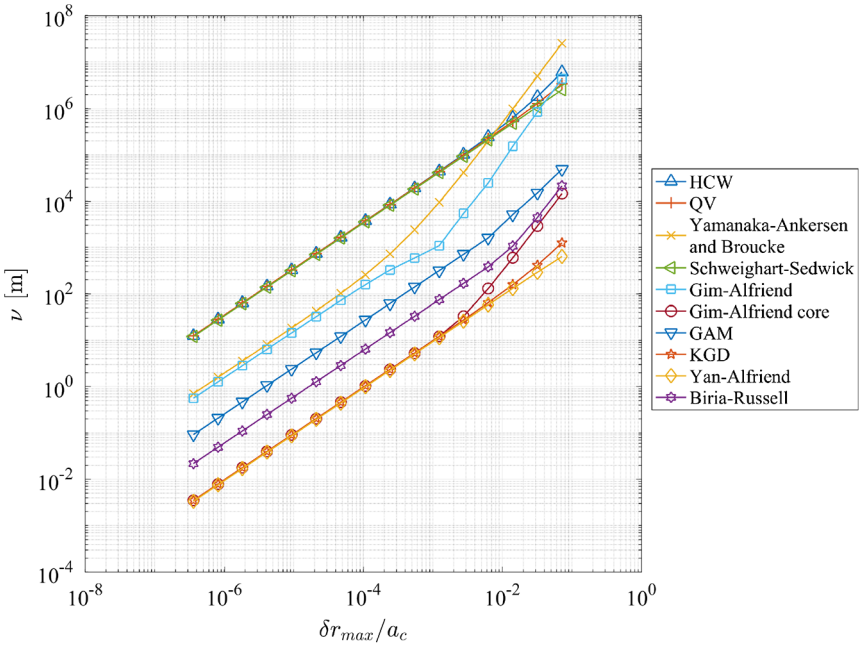

Fig. 11 Scenario 3 modeling error compared with J_2–J_5 truth.

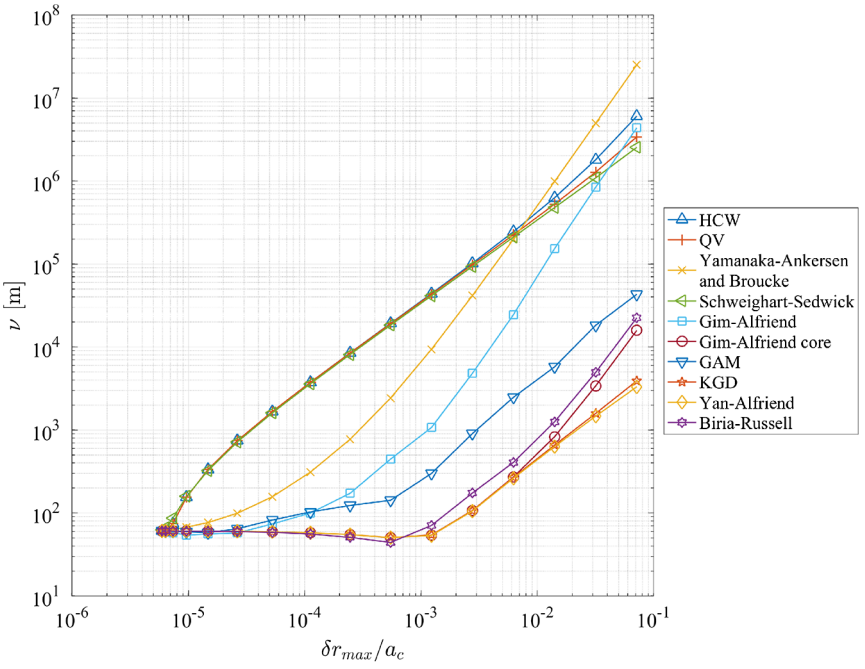

Fig. 12 Scenario 3 modeling error compared with full-force truth.

using the Broucke or Yamanaka–Ankersen solutions over the Schweighart–Sedwick, quadratic Volterra, and curvilinear HCW models is particularly evident at smaller separations. However, as the interspacecraft separation is increased, the Broucke and Yamanaka–Ankersen propagation accuracy degrades more rapidly than the curvilinear HCW and quadratic Volterra methods. This is largely due to the fact that the former two models are implemented using rectilinear coordinates, whereas the curvilinear coordinates of the HCW model and the second-order rectilinear terms of the quadratic Volterra solution enable improved propagation accuracy at larger separations.

4. *Runtime Comparison*

The average wall-clock runtime for each model to propagate the relative motion for 24 h at 10 s outputs is computed and tabulated in Table 4. The runtimes for the analytic propagations are compared to the numerical integration, which also implements a 10 s step size. A distinction is made between the numerical integration of the equations of motion subject only to Earth's gravity field and the high-fidelity full-force model numerical integration including several other perturbing force models, which runs considerably slower. The runtime information for the Biria–Russell Vinti model was not available because the implementation was only made available as a MATLAB code, and thus it would be unfair to compare to the precompiled C++ implementations of the other closed-form models. All testing was performed on a system equipped with an Intel Core i7 four-core 4.00 GHz processor.

Clearly, the use of closed-form solutions drastically decreases the computational effort required for relative state propagation compared to numerical integration methods. Moreover, the models with simpler analytic forms, like the HCW solution, offer the fastest runtime with the tradeoff of generally lower propagation accuracies. Because the

Table 4 Runtime comparison of dynamics models for a 24 h simulation duration

Model	Runtime, s	Percent of truth model 1 and 2 numerical integration	Percent of truth model 3 numerical integration
Yan–Alfriend	0.0473	2.244	0.0907
HCW	0.0508	2.412	0.0975
Schweighart–Sedwick	0.0525	2.492	0.1007
Broucke	0.0610	2.896	0.1170
Quadratic Volterra	0.0659	3.131	0.1265
Yamanaka–Ankersen	0.0728	3.456	0.1396
GAM	0.0816	3.874	0.1565
Gim–Alfriend core	0.1063	5.050	0.2040
KGD	0.1308	6.210	0.2509
Gim–Alfriend	0.3186	15.13	0.6112
Biria–Russell	— —	— —	— —

nonlinear transformations from mean orbital element space to relative Cartesian state were not considered as part of a models propagation time, the orbital element-based models offer low computational efforts to propagate the mean relative state. Finally, it can be concluded that the propagation time increases drastically for models requiring the computation of a complex STM at each time step from the relatively high runtimes of the KGD and Gim–Alfriend models.

VII. Conclusions

It is certainly evident that there is a wide breadth of existing research on relative motion dynamics present in the literature. This survey has sought to capture relevant features of a large subset of this literature by assessing the choice of relative motion state parameterization, derivation methodology, fundamental assumptions on reference orbit eccentricity and interspacecraft separation, and the ability to incorporate perturbations into analytical solutions. As opposed to treating the models as independent of one another, it is shown that a proper consideration of several methods for interrepresentation mapping merges the benefits of multiple approaches, leading to a more complete understanding of the relative motion dynamics. Furthermore, the results of a simulation-based comparative assessment quantify several key features of the considered dynamics models. First, in all cases, the use of orbital element-based models enables a more effective linearization of the relative motion for larger ranges of validity and improved performance in environments with large differential disturbance accelerations because the inclusion of relevant secular perturbation effects is simpler. Second, it is clear that neglecting reference orbit eccentricity can result in significant propagation error, even if relevant perturbations such as J_2 are modeled. Finally, even though a majority of the evaluated models consider at least the dominant J_2 perturbation effect to some degree, there is a strong motivation for further inclusion of other relevant perturbations into closed-form dynamics models.

Appendix A: Summary of Surveyed Models

Note the following acronyms for Table A1: (non)-linear equations of relative motion [(N)LERM]; (quasi)-nonsingular [(Q)NS]; mean OED (MOED); Earth oblateness (J_2); atmospheric drag (AD); thrust maneuver (TM); solar radiation pressure (SRP); and third-body sun and moon (3B).

Appendix B: Mappings Between Representations

The following section serves as a reference for several of the surveyed nonlinear and linear state mappings.

B1. Maps Between Rectilinear and Spherical States

This section highlights the nonlinear mapping between the rectilinear relative position and velocity, $(\boldsymbol{\rho}, \dot{\boldsymbol{\rho}})^T$, and the spherical curvilinear relative position and velocity, $(\delta r, \theta, \phi, \delta\dot{r}, \dot{\theta}, \dot{\phi})^T$. Here, $\dot{\boldsymbol{\rho}} \triangleq {}^{\mathcal{R}}\mathrm{d}\boldsymbol{\rho}/\mathrm{d}t$ refers to relative velocity with derivative taken in the rotating chief RTN frame, δr denotes the difference in deputy and chief radius, θ is the angle between the projection of the deputy position vector on the chief orbital plane and the chief position vector, and ϕ is the angle between the deputy position vector and the chief orbital plane. The map from spherical to rectilinear state is given by

$$
\begin{aligned}
x &= (r_c + \delta r)\cos\theta\cos\phi - r_c \\
y &= (r_c + \delta r)\sin\theta\cos\phi \\
z &= (r_c + \delta r)\sin\phi \\
\dot{x} &= \delta\dot{r}\cos\theta\cos\phi - (r_c + \delta r)(\dot{\theta}\sin\theta\cos\phi + \dot{\phi}\cos\theta\sin\phi) \\
\dot{y} &= \delta\dot{r}\sin\theta\cos\phi + (r_c + \delta r)(\dot{\theta}\cos\theta\cos\phi - \dot{\phi}\sin\theta\sin\phi) \\
\dot{z} &= \delta\dot{r}\sin\phi + (r_c + \delta r)\dot{\phi}\cos\phi
\end{aligned} \tag{B1}
$$

The inverse map from rectilinear to spherical state is given by

$$
\begin{aligned}
\delta r &= \sqrt{(r_c + x)^2 + y^2 + z^2} - r_c \\
\theta &= \arctan\left(\frac{y}{r_c + x}\right) \\
\phi &= \arcsin\left(\frac{z}{\sqrt{(r_c + x)^2 + y^2 + z^2}}\right) \\
\delta\dot{r} &= \frac{(r_c + x)\dot{x} + y\dot{y} + z\dot{z}}{\sqrt{(r_c + x)^2 + y^2 + z^2}} \\
\dot{\theta} &= \frac{(r_c + x)\dot{y} - y\dot{x}}{(r_c + x)^2 + y^2} \\
\dot{\phi} &= \frac{(r_c + \delta r)\dot{z} - z\delta\dot{r}}{(r_c + \delta r)\sqrt{(r_c + \delta r)^2 - z^2}}
\end{aligned} \tag{B2}
$$

Vallado [85] provides an excellent resource for additional curvilinear states and their associated mappings.

B2. Maps Between Hill–Clohessy–Wiltshire Invariant Parameters and Relative Position and Velocity

In [14,15], the authors define a relative state built from the integration constants of the HCW solution, $\delta\boldsymbol{x} = (a_e, x_d, y_d, \beta, z_{\max}, \psi)^T$. The definition of these HCW invariant parameters in terms of the translational states $(\boldsymbol{\rho}, \dot{\boldsymbol{\rho}})^T$ is given by

$$
\begin{aligned}
a_e &= 2\sqrt{\left(\frac{\dot{x}}{n}\right)^2 + \left(3x + 2\frac{\dot{y}}{n}\right)^2} \\
x_d &= 4x + 2\frac{\dot{y}}{n} \\
y_d &= y - 2\frac{\dot{x}}{n} \\
\beta &= \tan^{-1}(\dot{x}, 3nx + 2\dot{y}) \\
z_{\max} &= \sqrt{\left(\frac{\dot{z}}{n}\right)^2 + z^2} \\
\psi &= \tan^{-1}(nz, \dot{x})
\end{aligned} \tag{B3}
$$

where n is the mean motion of the chief. The two-argument arctangent is used to ensure the correct quadrant of β and ψ when taking the inverse. Also, note that $\dot{\boldsymbol{\rho}} \triangleq {}^{\mathcal{R}}\mathrm{d}\boldsymbol{\rho}/\mathrm{d}t$ defines the relative velocity with derivative taken in the rotating chief RTN frame.

The inverse map from the newly defined parameters to the relative translational state is

Table A1 Categorized summary of surveyed relative dynamics models

		Modeling assumptions			
References	State	Orbit regime	Solution form	Perturbations	Model description
[6]	Relative position and velocity	Any e	Equations of motion	General	Derives general NLERM [Eq. (1)] subject to arbitrary differential perturbations in the chief RTN frame.
[6,7,13]	Relative position and velocity	Near-circular	Linear	None	Derives HCW LERM [7]. Applies STM for rectilinear [6] and curvilinear [6,13] state propagation.
[14,15]	HCW invariants	Near-circular	Linear	None	State using integration constants of HCW solution for improved relative orbit geometry insight and control design.
[18,19]	Relative position and velocity	Near-circular	Linear	J_2, AD	Extension of HCW model to include first-order J_2 effects. First-order AD effects additionally considered in [19].
[22,23]	Relative position and velocity	Near-circular	Linear	AD	Adds linear drag [22] and then quadratic drag [23] to HCW. Assumes inverse density model and equal drag coefficients.
[24]	Relative position and velocity	Near-circular	Linear	J_2, AD	Extends model of [18] to included analytical effect of atmospheric drag for formation control.
[25]	HCW invariants	Near-circular	Linear	TM	Develops closed-form extension of [14,15] to include continuous thrust maneuvers designed using input shaping.
[26]	HCW invariants	Near-circular	Linear	AD	Extends model in [14,15] to include AD perturbation by developing variational equations for the state parameters.
[28]	Relative position and velocity	Near-circular	Nonlinear	None	Compares the QV (rectilinear), MS (spherical), DT, and A-DT (curvilinear) nonlinear dynamics models.
[29]	Relative position and velocity	Near-circular	Nonlinear (open)	J_2	Develops a framework for including J_2 in QV nonlinear model, but does not derive closed-form solution.
[31,32]	Relative position and velocity	Any e	Equations of motion	None	Derives the Lawden/Tschauner–Hempel LERM.
[33]	Relative position and velocity	Any e	Linear	None	Carter's development of singularity-free STM solution to TH equations. Noteworthy computational complexity.
[34]	Relative position and velocity	Any e	Linear	None	Derives and validates the Yamanaka–Ankersen STM for solving TH equations. Tested with e_c as high as 0.7.
[37]	Relative position and velocity	Any e	Linear	None	Melton's time-explicit STM built from recursive integrals in expanding powers of e_c. Model retains $\mathcal{O}(e_c^2)$ terms.
[38]	Relative position and velocity	Any e	Linear	None	Time-explicit model using the analytical two-body solution to write a STM as a variation of chief orbital parameters.
[40]	Relative position and velocity	Any e	Linear	None	Derives time-explicit Lee–Cochran–Jo STM using linear map between relative state and variation in chief state.
[41,42]	Relative position and velocity	Any e	Equations of motion	J_2, AD, TM	Derives NLERM subject to multiple differential perturbations. No closed-form solutions obtained.
[44–46]	MOED	Any e	Linear	J_2	State using Delaunay OED to characterize relative orbits with zero OED drift to first-order (J_2-invariant).
[47,49]	QNS MOED and NS MOED	Any e	Linear	J_2	Derives STM in QNS MOED [47] and NS MOED [49] using Brouwer theory to capture $\mathcal{O}(J_2)$ secular effects.
[52]	Singular, QNS, and NS ROE	Any e	Linear	J_2, AD	Develops a general procedure using GVE and Floquet theory to include multiple perturbations in compact STM.
[53,54]	MOED	Any e	Nonlinear	J_2	Derives model that expands deputy OE to second order about chief and retains $\mathcal{O}(J_2^2)$ perturbation effects.
[58–60]	Relative E/I-vector ROE	Near-circular	Linear	J_2	Establishes E/I-vector separation for formation design and passive safety and develops J_2-perturbed STM.
[63]	Relative E/I-vector ROE	Near-circular	Linear	J_2, AD	Improves J_2 STM of [60] by including secular effects due to relative semimajor axis. Time-varying drag is included.
[69]	Relative E/I-vector ROE	Near-circular (GEO)	Linear	J_2, AD, SRP, 3B	Propagates the ROE subject to J_2 and AD using STM from [63] and adds effects of SRP and 3B.
[80]	Euler parameters	Any e	Variational equations	General	Reformulates the DCM from perifocal to orbit-fixed frame using quaternions. Derives modified nonsingular LPE.
[81]	Epicyclic parameters	Near-circular	Linear	J_2	Derives canonical parameters from unperturbed Hamiltonian. Uses variation of parameters to capture J_2.
[82]	Spheroidal orbital elements	Any e	Linear	J_2, J_3, partial J_4	Uses Vinti-based (instead of Brouwer-based) approach to derive STM capturing higher-order geopotential effects.

$$
\begin{aligned}
x &= -\frac{a_e}{2}\cos\beta + x_d \\
y &= a_e \sin\beta + y_d \\
z &= z_{\max}\sin\psi \\
\dot{x} &= \frac{a_e}{2} n \sin\beta \\
\dot{y} &= a_e n \cos\beta - \frac{3}{2} n x_d \\
\dot{z} &= z_{\max} n \cos\psi
\end{aligned} \tag{B4}
$$

B3. Exact Nonlinear Map from Keplerian Orbital Elements to Relative Position

The exact nonlinear mapping between chief and deputy Keplerian orbital elements, $\boldsymbol{\alpha} = (a, e, i, \Omega, \omega, f)^T$, and the relative position in RTN coordinates $\boldsymbol{\rho}$ is derived in Gurfil and Kholshevnikov [72] as

$$
\begin{aligned}
x &= \frac{1}{2}[(k_3 - k_2)\sin(f_c - E_d) + (k_1 + k_4)\cos(f_c - E_d) \\
&\quad + (k_3 + k_2)\sin(f_c + E_d) + (k_1 - k_4)\cos(f_c + E_d)] \\
&\quad - e_d(k_3 \sin f_c + k_1 \cos f_c) - r_c \\
y &= \frac{1}{2}[-(k_1 + k_4)\sin(f_c - E_d) + (k_3 - k_2)\cos(f_c - E_d) \\
&\quad + (k_4 - k_1)\sin(f_c + E_d) + (k_2 + k_3)\cos(f_c + E_d)] \\
&\quad + e_d(k_1 \sin f_c - k_3 \cos f_c) \\
z &= k_5(\cos E_d - e_d) + k_6 \sin E_d
\end{aligned} \tag{B5}
$$

To simplify the equations of motion, the authors introduce a relative RAAN Ω^*, relative argument of periapsis ω^*, and relative inclination i^*. They are defined by expressing the product of the rotation matrices from the deputy perifocal frame P_d to the inertial frame I and the inertial frame to the chief perifocal frame P_c as a single rotation matrix, composed from the 3-1-3 rotation sequence from deputy perifocal frame to chief perifocal frame by angles $-\omega^*$, $-i^*$, and $-\Omega^*$, respectively. Mathematically, the angles are found by solving

$$
\boldsymbol{R}_{P_d}^{P_c}(\Omega^*, i^*, \omega^*) = \boldsymbol{R}_I^{P_c}(\Omega_c, i_c, \omega_c)\boldsymbol{R}_{P_d}^{I}(\Omega_d, i_d, \omega_d) \tag{B6}
$$

Figure 6.1 of [6] depicts the newly defined angles in Earth-centered inertial frame. The parameters k_i are defined by

$$
\begin{aligned}
k_1 &= a_d(\cos\Omega^* \cos\omega^* - \sin\Omega^* \sin\omega^* \cos i^*) \\
k_2 &= b_d(-\cos\Omega^* \sin\omega^* - \sin\Omega^* \cos\omega^* \cos i^*) \\
k_3 &= a_d(\sin\Omega^* \cos\omega^* + \cos\Omega^* \sin\omega^* \cos i^*) \\
k_4 &= b_d(-\sin\Omega^* \sin\omega^* + \cos\Omega^* \cos\omega^* \cos i^*) \\
k_5 &= a_d \sin\omega^* \sin i^* \\
k_6 &= b_d \cos\omega^* \sin i^*
\end{aligned} \tag{B7}
$$

Last, the conic section relationships

$$
\begin{aligned}
r &= \frac{a(1 - e^2)}{1 - e\cos f} \\
b_d &= a_d\sqrt{1 - e_d^2}
\end{aligned} \tag{B8}
$$

are used in the equations for the nonlinear mapping.

B4. Nonlinear Unit Sphere Mapping from Orbital Elements to Relative Position and Velocity

Vadali's nonlinear unit sphere approach [74] expresses the normalized relative position components as functions of the chief and deputy RAAN, inclination, argument of latitude, and their differences, $\Delta(\cdot) = (\cdot)_d - (\cdot)_c$. The argument of latitude is expressed as $\theta = \omega + f$. The formula for the normalized relative position components are

$$
\begin{aligned}
\tilde{x} &= -1 + \cos^2\frac{i_c}{2}\cos^2\frac{i_d}{2}\cos(\Delta\theta + \Delta\Omega) \\
&\quad + \sin^2\frac{i_c}{2}\sin^2\frac{i_d}{2}\cos(\Delta\theta - \Delta\Omega) \\
&\quad + \sin^2\frac{i_c}{2}\cos^2\frac{i_d}{2}\cos(2\theta_c + \Delta\theta + \Delta\Omega) \\
&\quad + \cos^2\frac{i_c}{2}\sin^2\frac{i_d}{2}\cos(2\theta_c + \Delta\theta - \Delta\Omega) \\
&\quad + \frac{1}{2}\sin i_c \sin i_d[\cos\Delta\theta - \cos(2\theta_c + \Delta\theta)] \\
\tilde{y} &= \cos^2\frac{i_c}{2}\cos^2\frac{i_d}{2}\sin(\Delta\theta + \Delta\Omega) + \sin^2\frac{i_c}{2}\sin^2\frac{i_d}{2}\sin(\Delta\theta - \Delta\Omega) \\
&\quad - \sin^2\frac{i_c}{2}\cos^2\frac{i_d}{2}\sin(2\theta_c + \Delta\theta + \Delta\Omega) \\
&\quad - \cos^2\frac{i_c}{2}\sin^2\frac{i_d}{2}\sin(2\theta_c + \Delta\theta - \Delta\Omega) \\
&\quad + \frac{1}{2}\sin i_c \sin i_d[\sin\Delta\theta + \sin(2\theta_c + \Delta\theta)] \\
\tilde{z} &= -\sin i_c \sin\Delta\Omega\cos\theta_d \\
&\quad - (\sin i_c \cos i_d \cos\Delta\Omega - \cos i_c \sin i_d)\sin\theta_d
\end{aligned} \tag{B9}
$$

The actual relative position is obtained by scaling the normalized coordinates:

$$
\begin{aligned}
x &= r_d(1 + \tilde{x}) - r_c \\
y &= r_d\tilde{y} \\
z &= r_d\tilde{z}
\end{aligned} \tag{B10}
$$

The conic equation gives the radius of either spacecraft in terms of its osculating Keplerian orbital elements

$$
r = \frac{a(1 - e^2)}{1 + e\cos f} \tag{B11}
$$

Furthermore, the normalized relative position coordinates can be differentiated in the rotating reference frame and the exact relative velocity is obtained by the scaling

$$
\begin{aligned}
\dot{x} &= r_d\dot{\tilde{x}} + \dot{r}_d(1 + \tilde{x}) - \dot{r}_c \\
\dot{y} &= r_d\dot{\tilde{y}} + \dot{r}_d\tilde{y} \\
\dot{z} &= r_d\dot{\tilde{z}} + \dot{r}_d\tilde{z}
\end{aligned} \tag{B12}
$$

as noted in [6].

B5. Linear Map from Quasi-Nonsingular Orbital Element Difference to Relative Position and Velocity

The complete linear mapping between the relative state defined by the quasi-nonsingular OED, $\delta\boldsymbol{\alpha} = (\Delta a, \Delta\theta, \Delta i, \Delta q_1, \Delta q_2, \Delta\Omega)^T$, and the relative position and velocity state, $\delta\boldsymbol{x} = (\boldsymbol{\rho}, \dot{\boldsymbol{\rho}})^T$, is derived in [75]. The mapping to relative position is formulated as

$$
\begin{aligned}
x &= \frac{r_c}{a_c}\Delta a + \frac{V_r}{V_t} r_c \Delta\theta - \frac{r_c}{p_c}(2a_c q_{1,c} + r_c \cos\theta_c)\Delta q_1 \\
&\quad - \frac{r_c}{p_c}(2a_c q_{2,c} + r_c \sin\theta_c)\Delta q_2 \\
y &= r_c(\Delta\theta + \Delta\Omega \cos i_c) \\
z &= r_c(\Delta i \sin\theta_c - \Delta\Omega \cos\theta_c \sin i_c)
\end{aligned} \tag{B13}
$$

The mapping to relative velocity is formulated as

$$
\begin{aligned}
\dot{x} &= -\frac{V_r}{2a_c}\Delta a + \left(\frac{1}{r_c} - \frac{1}{p_c}\right) h_c \Delta\theta + \frac{1}{p_c}(V_r a_c q_{1,c} + h_c \sin\theta_c)\Delta q_1 \\
&\quad + \frac{1}{p_c}(V_r a_c q_{2,c} - h_c \cos\theta_c)\Delta q_2 \\
\dot{y} &= -\frac{2V_t}{2a_c}\Delta a - V_r \Delta\theta + \frac{1}{p_c}(3V_t a_c q_{1,c} + 2h_c \cos\theta_c)\Delta q_1 \\
&\quad + \frac{1}{p_c}(2V_t a_c q_{2,c} + 2h_c \sin\theta_c)\Delta q_2 + V_r \Delta\Omega \cos i_c \\
\dot{z} &= (V_t \cos\theta_c + V_r \sin\theta_c)\Delta i \\
&\quad + (V_t \sin\theta_c - V_r \cos\theta_c)\Delta\Omega \sin i_c
\end{aligned} \tag{B14}
$$

The well-known geometric and kinematic relationships

$$
\begin{aligned}
r &= \frac{a(1 - q_1^2 - q_2^2)}{1 + q_1 \cos\theta + q_2 \sin\theta} \\
p &= a(1 - q_1^2 - q_2^2) \\
h &= \sqrt{\mu p} \\
V_r &= \dot{r} = \frac{h}{p}(q_1 \sin\theta - q_2 \cos\theta) \\
V_t &= r\dot{\theta} = \frac{h}{p}(1 + q_1 \cos\theta + q_2 \sin\theta)
\end{aligned} \tag{B15}
$$

are used, with the true argument of latitude denoted as θ. This mapping is used in development of the Gim–Alfriend STM in [47] to map the osculating quasi-nonsingular OED propagation to the relative translational state. Note that $\dot{\boldsymbol{\rho}} \triangleq {}^{\mathcal{R}}\mathrm{d}\boldsymbol{\rho}/\mathrm{d}t$ refers to the relative velocity with derivative taken in the rotating chief RTN frame.

B6. Linear Map from Keplerian Orbital Element Difference to Relative Position

In [43], the linear mapping between the classical Keplerian OED relative state, $\delta\boldsymbol{\alpha} = (\Delta a, \Delta M, \Delta i, \Delta\omega, \Delta e, \Delta\Omega)^T$, and relative position $\boldsymbol{\rho}$ is given for arbitrarily eccentric orbits as

$$
\begin{aligned}
x &= \frac{r_c}{a_c}\Delta a + \frac{a_c e_c \sin f_c}{\eta_c}\Delta M - a_c \Delta e \cos f_c \\
y &= \frac{r_c}{\eta_c^3}(1 + e_c \cos f_c)^2 \Delta M + r_c \Delta\omega \\
&\quad + \frac{r_c \sin f_c}{\eta_c^2}(2 + e_c \cos f_c)\Delta e + r_c \Delta\Omega \cos i_c \\
z &= r_c(\Delta i \sin\theta_c - \Delta\Omega \cos\theta_c \sin i_c)
\end{aligned} \tag{B16}
$$

The true anomaly is given by f, the quantity $\theta = \omega + f$ is the true argument of latitude, and $\eta = \sqrt{1 - e^2}$ is an alternative way of expressing the eccentricity. Additionally, the conic equation in the form

$$
r = \frac{a\eta^2}{1 + e \cos f} \tag{B17}
$$

is used to complete the mapping. The velocity components of this mapping can be obtained either by differentiating Eq. (B16) in the rotating chief RTN frame with respect to time or by rewriting the quasi-nonsingular OED in Eq. (B14) as functions of the classical Keplerian OED.

B7. Linear Map from E/I-Vector Relative Orbital Elements to Relative Position and Velocity

Using the ROE state based on the relative eccentricity and inclination vectors, $\delta\boldsymbol{\alpha} = (\delta a, \delta\lambda, \delta e_x, \delta e_y, \delta i_x, \delta i_y)^T$, [59,60,79] derive the linear mapping between $\delta\boldsymbol{\alpha}$ and the relative position and velocity, $(\boldsymbol{\rho}, \dot{\boldsymbol{\rho}})^T$, for near-circular orbits. Here, $u = \omega + M$ is the mean argument of latitude:

$$
\begin{aligned}
x/a_c &= \delta a - \delta e_x \cos u_c - \delta e_y \sin u_c \\
y/a_c &= -\tfrac{3}{2}\delta a u_c + \delta\lambda + 2\delta e_x \sin u_c - 2\delta e_y \cos u_c \\
z/a_c &= \delta i_x \sin u_c - \delta i_y \cos u_c \\
\dot{x}/n_c a_c &= \delta e_x \sin u_c - \delta e_y \cos u_c \\
\dot{y}/n_c a_c &= -\tfrac{3}{2}\delta a + 2\delta e_x \cos u_c + 2\delta e_y \sin u_c \\
\dot{z}/n_c a_c &= \delta i_x \cos u_c + \delta i_y \sin u_c
\end{aligned} \tag{B18}
$$

Note that the relative position and velocity components on the left side of the equations can be interpreted either as rectilinear or (more accurately) as curvilinear quantities, and the velocity represents a derivative with respect to time taken in the rotating chief RTN frame.

Acknowledgments

This work was supported as part of the U.S. Air Force Research Laboratory's Control, Navigation, and Guidance for Autonomous Spacecraft project under contract FA9453-16-C-0029. The authors are thankful for their support. In addition, the authors would like to thank Ashley Biria as well as S. A. Schweighart, K. T. Alfriend, and H. Yan for providing validation code to support the implementation of their respective dynamics models for the assessment.

References

[1] Scharf, D. P., Hadaegh, F. Y., and Ploen, S. R., "A Survey of Spacecraft Formation Flying Guidance and Control (Part 1): Guidance," *Proceedings of the 2003 American Control Conference*, IEEE Publ., Piscataway, NJ, 2003, pp. 1733–1739.

[2] Scharf, D. P., Hadaegh, F. Y., and Ploen, S. R., "A Survey of Spacecraft Formation Flying Guidance and Control (Part 2): Control," *Proceedings of the 2004 American Control Conference*, IEEE Publ., Piscataway, NJ, 2004, pp. 2976–2985.

[3] Alfriend, K. T., and Yan, H., "Evaluation and Comparison of Relative Motion Theories," *Journal of Guidance, Control, and Dynamics*, Vol. 28, No. 2, 2005, pp. 254–261. doi:10.2514/1.6691

[4] Russell, R., "Survey of Spacecraft Trajectory Design in Strongly Perturbed Environments," *Journal of Guidance, Control, and Dynamics*, Vol. 35, No. 3, 2012, pp. 705–720. doi:10.2514/1.56813

[5] Quadrelli, M. B., Wood, L. J., Riedel, J. E., McHenry, M. C., Aung, M., Cangahuala, L. A., Volpe, R. A., Beauchamp, P. M., and Cutts, J. A., "Guidance, Navigation, and Control Technology Assessment for Future Planetary Science Missions," *Journal of Guidance, Control, and Dynamics*, Vol. 38, No. 7, 2015, pp. 1165–1186. doi:10.2514/1.G000525

[6] Alfriend, K., Vadali, S. R., Gurfil, P., How, J., and Breger, L., *Spacecraft Formation Flying: Dynamics, Control and Navigation*, Vol. 2, Butterworth Heinemann, Burlington, MA, 2009, pp. 25–28, 60–64, 99–103, 125, 145, 150.

[7] Clohessy, W. H., and Wiltshire, R. S., "Terminal Guidance System for Satellite Rendezvous," *Journal of the Aerospace Sciences*, Vol. 27, No. 9, 1960, pp. 653–658. doi:10.2514/8.8704

[8] Chamberlin, J. A., and Rose, J. T., "Gemini Rendezvous Program," *Journal of Spacecraft and Rockets*, Vol. 1, No. 1, 1964, pp. 13–18. doi:10.2514/3.27585

[9] Aldrin, B., "Line-of-Sight Guidance Techniques for Manned Orbital Rendezvous," Ph.D. Thesis, Massachusetts Inst. of Technology, Cambridge, MA, 1963.

[10] Goodman, J. L., "History of Space Shuttle Rendezvous and Proximity Operations," *Journal of Spacecraft and Rockets*, Vol. 43, No. 5, 2006, pp. 944–959. doi:10.2514/1.19653

[11] Davis, T. M., and Melanson, D., "XSS-10 Microsatellite Flight Demonstration Program Results," *Proceedings of the Spacecraft Platforms and Infrastructure Conference*, SPIE — The International Soc. for Optics and Photonics, Bellingham, WA, 2004, pp. 16–25. doi:10.1117/12.544316

[12] Kawano, I., Mokuno, M., Kasai, T., and Suzuki, T., "First Autonomous Rendezvous Using Relative GPS Navigation by ETS-VII," *Journal of the Institute of Navigation*, Vol. 48, No. 1, 2001, pp. 49–56. doi:10.1002/navi.2001.48.issue-1

[13] De Bruijn, F., Gill, E., and How, J., "Comparative Analysis of Cartesian and Curvilinear Clohessy–Wiltshire Equations," *Journal of Aerospace Engineering, Sciences and Applications*, Vol. 3, No. 2, 2011, pp. 1–15. doi:10.7446/jaesa

[14] Lovell, T. A., and Tragesser, S., "Guidance for Relative Motion of Low Earth Orbit Spacecraft Based on Relative Orbit Elements," *AIAA/AAS Astrodynamics Specialist Conference and Exhibit*, AIAA Paper 2004-4988, Aug. 2004. doi:10.2514/6.2004-4988

[15] Chavez, F., and Lovell, T., "Relative-Orbit Element Estimation for Satellite Navigation and Guidance," *AIAA/AAS Astrodynamics Specialist Conference and Exhibit*, AIAA Paper 2004-5214, Aug. 2004. doi:10.2514/6.2004-5214

[16] Ichikawa, A., and Ichimura, Y., "Optimal Impulsive Relative Orbit Transfer Along a Circular Orbit," *Journal of Guidance, Control, and Dynamics*, Vol. 31, No. 4, 2008, pp. 1014–1027. doi:10.2514/1.32820

[17] Healy, L. M., and Henshaw, C. G., "Trajectory Guidance Using Periodic Relative Orbital Motion," *Journal of Guidance, Control, and Dynamics*, Vol. 38, No. 9, 2015, pp. 1714–1724. doi:10.2514/1.G000945

[18] Schweighart, S. A., and Sedwick, R. J., "High-Fidelity Linearized J_2 Model for Satellite Formation Flight," *Journal of Guidance, Control, and Dynamics*, Vol. 25, No. 6, 2002, pp. 1073–1080. doi:10.2514/2.4986

[19] Izzo, D., Sabatini, M., and Valente, C., "A New Linear Model Describing Formation Flying Dynamics Under J_2 Effects," *Proceedings of the 17th AIDAA Congress*, Rome, 2003, pp. 493–500.

[20] Izzo, D. R., "Formation Flying Linear Modelling," *Proceedings of the Dynamics and Controls of Systems and Structures in Space Conference*, Cambridge, U.K., July 2002, pp. 283–289.

[21] Leonard, C. L., Hollister, W. M., and Bergmann, E. V., "Orbital Formationkeeping with Differential Drag," *Journal of Guidance, Control, and Dynamics*, Vol. 12, No. 1, 1989, pp. 108–113. doi:10.2514/3.20374

[22] Humi, M., and Carter, T., "Rendezvous Equations in a Central-Force Field with Linear Drag," *Journal of Guidance, Control, and Dynamics*, Vol. 25, No. 1, 2002, pp. 74–79. doi:10.2514/2.4851

[23] Carter, T., and Humi, M., "Clohessy–Wiltshire Equations Modified to Include Quadratic Drag," *Journal of Guidance, Control, and Dynamics*, Vol. 25, No. 6, 2002, pp. 1058–1063. doi:10.2514/2.5010

[24] Bevilacqua, R., and Romano, M., "Rendezvous Maneuvers of Multiple Spacecraft Using Differential Drag Under J_2 Perturbation," *Journal of Guidance, Control, and Dynamics*, Vol. 31, No. 6, 2008, pp. 1595–1607. doi:10.2514/1.36362

[25] Bevilacqua, R., and Lovell, T. A., "Analytical Guidance for Spacecraft Relative Motion Under Constant Thrust Using Relative Orbit Elements," *Acta Astronautica*, Vol. 102, Oct. 2014, pp. 47–61. doi:10.1016/j.actaastro.2014.05.004

[26] Bennett, T., and Schaub, H., "Continuous-Time Modeling and Control Using Nonsingular Linearized Relative-Orbit Elements," *Journal of Guidance, Control, and Dynamics*, Vol. 39, No. 12, 2016, pp. 2605–2614. doi:10.2514/1.G000366

[27] Colombo, O. L., "The Dynamics of Global Positioning System Orbits and the Determination of Precise Ephemerides," *Journal of Geophysical Research: Solid Earth*, Vol. 94, No. B7, 1989, pp. 9167–9182. doi:10.1029/JB094iB07p09167

[28] Newman, B. A., Sinclair, A. J., Lovell, A., and Perez, A., "Comparison of Nonlinear Analytical Solutions for Relative Orbital Motion," *AIAA/AAS Astrodynamics Specialist Conference*, AIAA Paper 2014-4163, 2014. doi:10.2514/6.2014-4163

[29] Stringer, M. T., Newman, B., Lovell, T. A., and Omran, A., "Analysis of a New Nonlinear Solution of Relative Orbital Motion," *Proceedings of the 23rd International Symposium on Space Flight Dynamics*, Jet Propulsion Lab., Pasadena, CA, 2012.

[30] Perez, A., Lovell, T. A., Geller, D., and Newman, B., "Relative Satellite Motion Solutions Using Curvilinear Coordinate Frames," *Proceedings of the AAS/AIAA Astrodynamics Specialist Conference*, AAS Paper 15-437, Vail, CO, 2015.

[31] Lawden, D. F., *Optimal Trajectories for Space Navigation*, Butterworths, Burlington, MA, 1963, p. 75.

[32] Tschauner, J., and Hempel, P., "Optimale Beschleunigungsprogramme fur das Rendezvous-Manover," *Astronautica Acta*, Vol. 10, Nos. 5–6, 1964, p. 296.

[33] Carter, T. E., "State Transition Matrices for Terminal Rendezvous Studies: Brief Survey and New Example," *Journal of Guidance, Control, and Dynamics*, Vol. 21, No. 1, 1998, pp. 148–155. doi:10.2514/2.4211

[34] Yamanaka, K., and Ankersen, F., "New State Transition Matrix for Relative Motion on an Arbitrary Elliptical Orbit," *Journal of Guidance, Control, and Dynamics*, Vol. 25, No. 1, 2002, pp. 60–66. doi:10.2514/2.4875

[35] Ardaens, J.-S., D'Amico, S., and Cropp, A., "GPS-Based Relative Navigation for the Proba-3 Formation Flying Mission," *Acta Astronautica*, Vol. 91, Nov. 2013, pp. 341–355. doi:10.1016/j.actaastro.2013.06.025

[36] Battin, R. H., *An Introduction to the Mathematics and Methods of Astrodynamics*, AIAA Education Series, AIAA, Reston, VA, 1999, Chaps. 4, 9.

[37] Melton, R. G., "Time-Explicit Representation of Relative Motion Between Elliptical Orbits," *Journal of Guidance, Control, and Dynamics*, Vol. 23, No. 4, 2000, pp. 604–610. doi:10.2514/2.4605

[38] Broucke, R. A., "Solution of the Elliptic Rendezvous Problem with the Time as Independent Variable," *Journal of Guidance, Control, and Dynamics*, Vol. 26, No. 4, 2003, pp. 615–621. doi:10.2514/2.5089

[39] de Vries, J. P., "Elliptic Elements in Terms of Small Increments of Position and Velocity Components," *AIAA Journal*, Vol. 1, No. 11, 1963, pp. 2626–2629. doi:10.2514/3.2124

[40] Lee, D., Cochran, J. E., and Jo, J. H., "Solutions to the Variational Equations for Relative Motion of Satellites," *Journal of Guidance, Control, and Dynamics*, Vol. 30, No. 3, 2007, pp. 669–678. doi:10.2514/1.24373

[41] Kechichian, J. A., "Motion in General Elliptic Orbit with Respect to a Dragging and Precessing Coordinate Frame," *Journal of the Astronautical Sciences*, Vol. 46, No. 1, 1998, pp. 25–45.

[42] Theron, A., Karai-Zaitri, M., Arzelier, D., and Louembert, C., "Nonlinear and Linear Local Cartesian Relative Motion State Models for J_2 Perturbed Elliptical Orbits," *Proceedings of the 21st International Symposium on Space Flight Dynamics*, University of Toulouse, Toulouse, France, 2009.

[43] Schaub, H., "Relative Orbit Geometry Through Classical Orbit Element Differences," *Journal of Guidance, Control, and Dynamics*, Vol. 27, No. 5, 2004, pp. 839–848. doi:10.2514/1.12595

[44] Schaub, H., and Alfriend, K. T., "J_2 Invariant Relative Orbits for Spacecraft Formations," *Celestial Mechanics and Dynamical Astronomy*, Vol. 79, No. 2, 2001, pp. 77–95. doi:10.1023/A:1011161811472

[45] Schaub, H., Vadali, S. R., Junkins, J. L., and Alfriend, K. T., "Spacecraft Formation Flying Control Using Mean Orbit Elements," *Journal of the Astronautical Sciences*, Vol. 48, No. 1, 2000, pp. 69–87.

[46] Schaub, H., and Alfriend, K. T., "Impulsive Feedback Control to Establish Specific Mean Orbit Elements of Spacecraft Formations," *Journal of Guidance, Control, and Dynamics*, Vol. 24, No. 4, 2001, pp. 739–745. doi:10.2514/2.4774

[47] Gim, D.-W., and Alfriend, K. T., "State Transition Matrix of Relative Motion for the Perturbed Noncircular Reference Orbit," *Journal of Guidance, Control, and Dynamics*, Vol. 26, No. 6, 2003, pp. 956–971. doi:10.2514/2.6924

[48] Brouwer, D., "Solution of the Problem of Artificial Satellite Theory Without Drag," *Astronomical Journal*, Vol. 64, Nov. 1959, p. 378. doi:10.1086/107958

[49] Gim, D.-W., and Alfriend, K. T., "Satellite Relative Motion Using Differential Equinoctial Elements," *Celestial Mechanics and*

Dynamical Astronomy, Vol. 92, No. 4, 2005, pp. 295–336.
doi:10.1007/s10569-004-1799-0

[50] Gim, D., and Alfriend, K., "Criteria for Best Configuration and Sub-Optimal Reconfiguration for MMS Mission," *Proceedings of the AAS Spaceflight Mechanics Meeting*, AAS Paper 04-152, Maui, HI, 2004.

[51] Roscoe, C. W. T., Westphal, J. J., Griesbach, J. D., and Schaub, H., "Formation Establishment and Reconfiguration Using Differential Elements in J_2-Perturbed Orbits," *Journal of Guidance, Control, and Dynamics*, Vol. 38, No. 9, 2015, pp. 1725–1740.
doi:10.2514/1.G000999

[52] Koenig, A., Guffanti, T., and D'Amico, S., "New State Transition Matrices for Relative Motion of Spacecraft Formations in Perturbed Orbits," *AIAA/AAS Astrodynamics Specialist Conference*, AIAA Paper 2016-5635, 2016.

[53] Alfriend, K., "Nonlinear Considerations in Satellite Formation Flying," *AIAA/AAS Astrodynamics Specialist Conference and Exhibit*, AIAA Paper 2002-4741, Aug. 2002.
doi:10.2514/6.2002-4741

[54] Alfriend, K. T., and Yan, H., "An Orbital Elements Based Approach to the Nonlinear Formation Flying Problem," *Proceedings of the International Formation Flying Conference: Missions and Technologies*, Toulouse, France, Oct. 2002.

[55] Eckstein, M., Rajasingh, C., and Blumer, P., "Colocation Strategy and Collision Avoidance for the Geostationary Satellites at 19 Degrees West," *Proceedings of the International Symposium on Space Flight Dynamics*, Vol. 6, Washington, D.C., 1989.

[56] Soop, E. M., *Handbook of Geostationary Orbits*, Vol. 3, Springer Science & Business Media, New York, 1994, Chap. 5.

[57] Arbinger, C., D'Amico, S., and Eineder, M., "Precise Ground-in-the-Loop Orbit Control for Low Earth Observation Satellites," *Proceedings of the 18th International Symposium on Space Flight Dynamics*, Vol. 548, Munich, 2004, p. 333.

[58] Montenbruck, O., Kirschner, M., D'Amico, S., and Bettadpur, S., "E/I-Vector Separation for Safe Switching of the GRACE Formation," *Aerospace Science and Technology*, Vol. 10, No. 7, 2006, pp. 628–635.
doi:10.1016/j.ast.2006.04.001

[59] D'Amico, S., and Montenbruck, O., "Proximity Operations of Formation-Flying Spacecraft Using an Eccentricity/Inclination Vector Separation," *Journal of Guidance, Control, and Dynamics*, Vol. 29, No. 3, 2006, pp. 554–563.
doi:10.2514/1.15114

[60] D'Amico, S., "Autonomous Formation Flying in Low Earth Orbit," Ph. D. Thesis, Delft Univ. of Technology, Delft, The Netherlands, 2010.

[61] Ardaens, J., D'Amico, S., and Fischer, D., "Early Flight Results from the TanDEM-X Autonomous Formation Flying System," *Proceedings of the 4th International Conference on Spacecraft Formation Flying Missions and Technologies (SFFMT)*, Saint-Hubert, QC, Canada, 2011.

[62] D'Amico, S., Ardaens, J.-S., and Larsson, R., "Spaceborne Autonomous Formation-Flying Experiment on the PRISMA Mission," *Journal of Guidance, Control, and Dynamics*, Vol. 35, No. 3, 2012, pp. 834–850.
doi:10.2514/1.55638

[63] Gaias, G., Ardaens, J.-S., and Montenbruck, O., "Model of J_2 Perturbed Satellite Relative Motion with Time-Varying Differential Drag," *Celestial Mechanics and Dynamical Astronomy*, Vol. 123, No. 4, 2015, pp. 411–433.
doi:10.1007/s10569-015-9643-2

[64] Spurmann, J., and D'Amico, S., "Proximity Operations of On-Orbit Servicing Spacecraft Using an Eccentricity/Inclination Vector Separation," *Proceedings of the 22nd International Symposium on Spaceflight Dynamics*, São José dos Campos, Brazil, 2011.

[65] Gaias, G., Ardaens, J.-S., and D'Amico, S., "The Autonomous Vision Approach Navigation and Target Identification (AVANTI) Experiment: Objectives and Design," *Proceedings of the 9th International ESA Conference on Guidance, Navigation & Control Systems*, Porto, Portugal, 2014.

[66] Gaias, G., D'Amico, S., and Ardaens, J.-S., "Generalised Multi-Impulsive Manoeuvres for Optimum Spacecraft Rendezvous in Near-Circular Orbit," *International Journal of Space Science and Engineering*, Vol. 3, No. 1, 2015, pp. 68–88.
doi:10.1504/IJSPACESE.2015.069361

[67] Gaias, G., and D'Amico, S., "Impulsive Maneuvers for Formation Reconfiguration Using Relative Orbital Elements," *Journal of Guidance, Control, and Dynamics*, Vol. 38, No. 6, 2015, pp. 1036–1049.
doi:10.2514/1.G000189

[68] Gaias, G., and Ardaens, J.-S., "Design Challenges and Safety Concept for the AVANTI Experiment," *Acta Astronautica*, Vol. 123, July 2016, pp. 409–419.
doi:10.1016/j.actaastro.2015.12.034

[69] Spiridonova, S., "Formation Dynamics in Geostationary Ring," *Celestial Mechanics and Dynamical Astronomy*, Vol. 125, No. 4, 2016, pp. 485–500.
doi:10.1007/s10569-016-9693-0

[70] Schaub, H., and Junkins, J. L., *Analytical Mechanics of Space Systems*, AIAA Education Series, AIAA, Reston, VA, 2003, Chap. 9.

[71] Sinclair, A. J., Sherrill, R. E., and Lovell, T. A., "Calibration of Linearized Solutions for Satellite Relative Motion," *Journal of Guidance, Control, and Dynamics*, Vol. 37, No. 4, 2014, pp. 1362–1367.
doi:10.2514/1.G000037

[72] Gurfil, P., and Kholshevnikov, K. V., "Manifolds and Metrics in the Relative Spacecraft Motion Problem," *Journal of Guidance, Control, and Dynamics*, Vol. 29, No. 4, 2006, pp. 1004–1010.
doi:10.2514/1.15531

[73] Gurfil, P., and Kasdin, N. J., "Nonlinear Modelling of Spacecraft Relative Motion in the Configuration Space," *Journal of Guidance, Control, and Dynamics*, Vol. 27, No. 1, 2004, pp. 154–157.
doi:10.2514/1.9343

[74] Vadali, S. R., "An Analytical Solution for Relative Motion of Satellites," *Proceedings of the 5th International Conference on Dynamics and Control of Structures in Space*, Cranfield Univ., Cranfield, England, U. K., July 2002, pp. 309–316.

[75] Schaub, H., and Alfriend, K. T., "Hybrid Cartesian and Orbit Element Feedback Law for Formation Flying Spacecraft," *Journal of Guidance, Control, and Dynamics*, Vol. 25, No. 2, 2002, pp. 387–393.
doi:10.2514/2.4893

[76] Alfriend, K. T., Gim, D.-W., and Schaub, H., "Gravitational Perturbations, Nonlinearity and Circular Orbit Assumption Effects on Formation Flying Control Strategies," *Proceedings of Guidance and Control 2000*, 2000, pp. 139–158.

[77] Anderson, P., and Schaub, H., "Impulsive Feedback Control of Nonsingular Elements in the Geostationary Regime," *AIAA/AAS Astrodynamics Specialist Conference*, AIAA Paper 2012-4585, Aug. 2012,
doi:10.2514/6.2012-4585

[78] Garrison, J. L., Gardner, T. G., and Axelrad, P., "Relative Motion in Highly Elliptical Orbits," *Advances in the Astronautical Sciences*, Vol. 89, 1995, pp. 1359–1376.

[79] D'Amico, S., "Relative Orbital Elements as Integration Constants of Hill's Equations," German Space Operations Center (GSOC) TN 05-08, Oberpfaffenhofen, Germany, 2005.

[80] Gurfil, P., "Euler Parameters as Nonsingular Orbital Elements in Near-Equatorial Orbits," *Journal of Guidance, Control, and Dynamics*, Vol. 28, No. 5, 2005, pp. 1079–1084.
doi:10.2514/1.14760

[81] Kasdin, N. J., and Kolemen, E., "Bounded, Periodic Relative Motion Using Canonical Epicyclic Orbital Elements," *Journal Advances in the Astronautical Sciences*, Vol. 120, No. 2, 2005, pp. 1381–1398.

[82] Biria, A., and Russell, R., "A Satellite Relative Motion Model Using J_2 and J_3 via Vinti's Intermediary," *AIAA/AAS Space Flight Mechanics Conference*, AAS Paper 16-537, Napa, CA, 2016.

[83] Gill, E., Montenbruck, O., and D'Amico, S., "Autonomous Formation Flying for the PRISMA Mission," *Journal of Spacecraft and Rockets*, Vol. 44, No. 3, 2007, pp. 671–681.
doi:10.2514/1.23015

[84] Junkins, J. L., Akella, M. R., and Alfriend, K. T., "Non-Gaussian Error Propagation in Orbital Mechanics," *Advances in the Astronautical Sciences*, Vol. 92, 1996, pp. 283–298.

[85] Vallado, D. A., *Fundamentals of Astrodynamics and Applications*, Vol. 12, 4th ed., Springer Science & Business Media, New York, 2001, Chap. 3.